

# Response to Reviewer#2 and Editor

(hess-2019-155)

Zhe Zhang, Yanping Li, Michael Barlage, Fei Chen, Gonzalo Miguez-Macho, Andrew Ireson, and Zhenhua Li

We appreciate the editor and two reviewers. They have put into time and effort to help us improve this article and their comments and suggestions are supportive and helpful. In the following text, the general response will be in red, original reviewers' comments and questions in *italic style* and our responses in [blue texts](#).

## Responses to Reviewer#2:

*Zhang et al. use a land surface model coupled to a two-way groundwater dynamics model to explore the response of groundwater to climate change in the Prairie Pothole Region (PPR) of North America. The study is worthwhile due to the need to explore the hydrologic response to climate change at the regional scale in the PPR.*

*The authors sufficiently addressed my technical concerns from the first round of revisions. However, some minor issues remain in the presentation of their study.*

*Line 51: what is "above soils" ?*

[Thank you for the question. In this context, the "above soils" was referred to the unsaturated soils which is above the saturated aquifer. We have changed to "subsurface soils" in the manuscript revision2, see L50-51.](#)

*Line 59: It would be better to actually review these studies included in the citation, as they support the idea that regional-scale simulation is necessary, and they have contributed important results to that end.*

[We really appreciate this idea and it is a good idea to review these cited papers, see L59-65. These papers are good examples that climate change and groundwater modeling studies are necessary because they are important for water management decision making. These cited papers also identify the limitation of previous studies in this area, such as poor groundwater representation in models and uncertainties in climate change projections.](#)

*Lines 71-75: ParFlow-CLM simulates three-dimensional flow in the unsaturated and saturated zone, two- dimension flow on the surface, and a two-way exchange between the surface and subsurface. Thus, I am not sure where the conclusion from Line 75 is coming from.*

[Thank you for correcting this confusion. In the cited paper \(Maxwell and Miller 2005\), CLM and ParFlow was coupled as a single-column model. We have changed the description. The more advanced features mentioned by the reviewer are reviewed in L78-81 and Maxwell et al. \(2015\) is cited.](#)

*Line 85: induce*

[Done](#)

*Line 137: Here you say 32 wells, but Figure 1 says 33.*  
Thank you. This should be 33.

*Line 141: formations*  
Done.

*Line 288: predicts a deep bias. (How deep is this bias?)*  
Deep bias about 5-m as in Fig. 6, see L297.

*Line 291: the water table*  
Done.

*Line 308: These hydrogeological*  
Done.

*Line 352: the current and future climate*  
Done.

*Line 356: rainfall events*  
Done.

*Figures 9&10: The authors claim in their response to have fixed the figure captions, but these still have captions that read “same as [previous figure].” These need to be rewritten to be descriptive and standalone.*  
Done.

*Figures 6&10: A color legend needs to be included on the figure for black, blue, and red lines. In addition, a label containing units for the central map color bar needs to be added.*  
Done. Thank you for the reminder. Legend and unit are added.

## **Responses to Editor:**

*Editor's comments:*

*Dear authors,*

*Thank you for your efforts to address the reviewer comments. These were mostly satisfactory. However, one of the reviewers had some additional comments and had noted that some changes had not been made. I had also found that some of the earlier changes that were said to be made had in fact not been made. Please go through the earlier referee reports and your responses to ensure that this is properly done. In addition, I have some minor comments (below). Please go through the entire manuscript for grammar as well.*

*P2, L21: the study does not consider mountainous regions. Change this to the northwestern part of the study area or something similar.*

[Done.](#)

*P2, L23: replace “bring forward” with “advancing”*

[Done.](#)

*P3, L40: add “the” in front of “freezing front”*

[Done.](#)

*P3, L41: remove the s from springs*

[Done.](#)

*P3, L45: remove the s from summers and falls*

[Done.](#)

*P4, L62: the objective of this paper “are” to...*

[Done.](#)

*On P4, the objectives are stated, but then the introduction and literature review continues after this. I recommend this be move toward the end of the section, as the second last paragraph.*

[Thank you for the recommendation. The objective paragraph has been moved to the second last paragraph in the introduction.](#)

*P5, L85: remove the s from induces*

[Done.](#)

*P5, L90: macropores “that” exist*

[Done.](#)

*P6, L 101: conduct dynamical downscaling. Also in L111.*

[Done. Thank you for the correction.](#)

*P6, L113: as follows*  
Done.

*P42, Fig. 6: a legend in the figure to show which line is simulation and which is observation would be helpful. Or else move the text from P16, L285–286 into the figure caption.*

Done. This is also mentioned by the reviewer#2. Thank you both for the correction, legend and unit are added.

*P18, L323: remove the s from rises*  
Done.

*P18, L329: fluxes show strong...*  
Done.

*P23, L412: we show that the model...*  
Done.

*P24, L450-451: fix the grammar with this sentence*  
Done.

*P26, L486: remove the s from components*  
Done.

*P26, L488: is challenging to what? A word is missing.*  
Done.

*P26, L490-491: please fix the grammar*  
Done. Thank you for the kind reminder.

1 **Modeling groundwater responses to climate change in the Prairie Pothole Region**

2

3

4

5

6 Zhe Zhang<sup>1</sup>, Yanping Li<sup>2</sup>, Michael Barlage<sup>3</sup>, Fei Chen<sup>3</sup>, Gonzalo Miguez-Macho<sup>3</sup>, Andrew Ireson<sup>4</sup>,

7

Zhenhua Li<sup>5</sup>

8

9

<sup>1</sup>*Global Institute for Water Security, University of Saskatchewan, Saskatoon, SK, Canada*

10

<sup>2</sup>*National Center for Atmospheric Research, Boulder, Colorado, USA*

11

<sup>3</sup>*Nonlinear Physic Group, Faculty of Physics, Universidade de Santiago de Compostela, Galicia, Spain*

12

13 Abstract

14 Shallow groundwater in the Prairie Pothole Region (PPR) is recharged predominantly by snowmelt  
15 in the spring and supplies water for evapotranspiration through the summer and fall. This two-way  
16 exchange is underrepresented in current land surface models. Furthermore, the impacts of climate  
17 change on the groundwater recharge rates are uncertain. In this paper, we use a coupled land and  
18 groundwater model to investigate the hydrological cycle of shallow groundwater in the PPR and  
19 study its response to climate change at the end of the 21st century. The results show that the model  
20 ~~does a reasonably good job of simulating the timing of recharge. The mean~~ water table depth  
21 ~~(WTD) is well simulated, except the model predicts deep WTD in northwestern Alberta.~~ The most  
22 significant change under future climate conditions occurs in the winter, when warmer temperature  
23 changes the rain/snow partitioning, delaying the time for snow accumulation/soil freezing while  
24 ~~advancing~~ early melting/thawing. Such changes lead to an earlier start to a longer recharge season,  
25 but with lower recharge rates. Different signals are shown in the eastern and western PPR in the  
26 future summer, with reduced precipitation and drier soils in the east but little change in the west.  
27 The annual recharge increased by 25% and 50% in the eastern and western PPR, respectively.  
28 Additionally, we found the mean and seasonal variation of the simulated WTD are sensitive to  
29 soil properties and fine-scale soil information is needed to improve groundwater simulation on  
30 regional scale.

31

32 Keywords: Groundwater, Recharge, Climate Change, Prairie Pothole Region, Hydrological Cycle,

**Deleted:** reasonably simulates the

**Deleted:** and the timing of recharge processes, but predicts deep WTD in mountainous region in Alberta

**Deleted:** bring forward

37 Introduction

38 The Prairie Pothole Region (PPR) in North America is located in a semi-arid and cold region,  
39 where evapotranspiration (ET) exceeds precipitation (PR) in summer and near-surface soil is  
40 frozen in winter (Gray, 1970; Granger and Gray, 1989; Hayashi et al., 2003; Pomeroy et al., 2007;  
41 Ireson et al., 2013; Dumanski et al., 2015). These climatic conditions have introduced unique  
42 hydrological characters to the groundwater flow in the PPR (Ireson et al., 2013). During winters,  
43 frozen soils reduce permeability and snow accumulates on the surface, prohibiting infiltration (Niu  
44 and Yang 2006; Mohammed et al., 2018). At the same time, the water table slowly declines due to  
45 a combination of upward transport to ~~the~~ freezing front by the capillary effect and discharge to  
46 rivers (Ireson et al., 2013). In early spring, snowmelt becomes the dominant component of the  
47 hydrological cycle and the melt water runs over frozen soil, with little infiltration contributing to  
48 recharge. As the soil thaws, the increased infiltration capacity allows snowmelt recharge to the  
49 water table, the previously upward water movement by capillary effect to reverse and move  
50 downwards, and the water table to rise to its maximum level. In summer, and fall, when high ET  
51 exceeds PR, capillary rise may draw water from the groundwater aquifers to supply ET demands,  
52 declining water table. These processes characterize the two-way water exchange between sub-  
53 surface soils and groundwater aquifers.

Deleted: s

Deleted: s

Deleted: s

54

55 Previous studies have suggested that substantial changes to groundwater interactions with ~~sub-~~  
56 ~~surface~~ soils are likely to occur under climate change (Tremblay et al., 2011; Green et al., 2011;  
57 Ireson et al., 2013, 2015). Existing modeling studies on the impacts of climate change on  
58 groundwater are either at global or basin/location-specific scales (Meixner et al., 2016). Global-  
59 level groundwater studies focus on potential future recharge trends (Doll and Fiedler, 2008; Doll,

Deleted: above

64 2009; Green et al., 2011), yet coarse resolution analysis from global climate models (GCMs)  
65 provided insufficient specificity to inform decision making. Basin-scale groundwater studies  
66 connect the climate with groundwater-flow models to understand the climate impacts on specific  
67 systems (Maxwell and Kollet, 2008; Kurylyk and MacQuarrie, 2013; Dumanski et al., 2015).  
68 Regional groundwater modeling studies, such as in the Colorado River Basin (Christensen et al.,  
69 2004) and in the western U.S. (Niraula et al., 2017), have applied downscaled climate scenarios  
70 from GCMs to drive large scale hydrology models. These studies identified research gaps  
71 associated with poor representation of groundwater-soil interactions in models and uncertainties  
72 in future climate projections.

73  
74 It is challenging to represent groundwater flows in LSMs because the important two-way water  
75 exchange between unsaturated soils and groundwater aquifers was neglected in previous LSMs.  
76 Recently, this two-way exchange has been implemented in coupled land surface – groundwater  
77 models (LSM-GW). For example, Maxwell and Miller (2005) used a groundwater model (ParFlow)  
78 coupled with the Common Land Model (CLM) as a single column model. They found that the  
79 coupled and uncoupled models were very similar in simulated sensible heat flux (SH), ET, and  
80 shallow soil moisture (SM), but differed greatly in simulated runoff and deep SM. Later on, Kollet  
81 and Maxwell (2008) incorporated the ET effect on redistributing moisture upward from shallow  
82 water table depth (WTD) and found the surface energy partitioning is highly sensitive to the WTD  
83 when the WTD is less than 5 m below ground surface. Niu et al. (2011) implemented a simple  
84 groundwater model (SIMGM, Niu et al., 2007), into the community Noah LSM with multi-  
85 parameterization options (Noah-MP LSM), by adding an unconfined aquifer at the bottom of soil  
86 layers. More complex features such as three-dimensional subsurface flow and two-dimensional

**Deleted:** However, a knowledge gap exists in predicting the effect of climate change over large regions (major river basins, states or group of states) (Christensen et al., 2004; Green et al., 2011; Niraula et al., 2017). ¶

Therefore, the objectives of this paper is to investigate the hydrological changes in groundwater in PPR under climate change and understand the drivers for different hydrological processes. Our goals are: 1) to model the water table dynamics in the PPR using a coupled land-groundwater model; 2) to capture changes in the groundwater regime under climate change; and 3) to identify major climatic and land surface processes that contribute to these changes in the PPR. ¶

**Deleted:** However, i

**Deleted:** modeling the

**Deleted:** PPR using

**Deleted:** is challenging

**Deleted:** is

**Deleted:** are different

**Deleted:** This is perhaps because only downwards flow from soil to groundwater is considered.

**Deleted:** partition

**Deleted:** a WTD ranging from 1 – 5 m

**Deleted:** More recently,

**Moved down [1]:** In Maxwell et al. (2015), m

**Deleted:** advanced



114 surface were included in ParFlow v3 and evaluated over much of continental North America for a  
115 very fine 1-km resolution (Maxwell et al., 2015). These recent development in coupled land and  
116 groundwater models have advanced our knowledge on the important interactions between soil and  
117 groundwater aquifer.

Deleted: have been developed

Deleted:

Moved (insertion) [1]

Deleted: In

Deleted: (

Deleted: )

Deleted: , m

119 In cold regions, soil freeze-thaw processes further complicate this two-way exchange. Field studies  
120 have found that frozen soil not only influences the timing and amount of downward recharge to  
121 aquifers by reducing the soil permeability (Koren et al., 1999; Niu et al., 2006; Kelln et al., 2007),  
122 but may also induce upward water transport from aquifers to soil freezing fronts (Spaans and Baker,  
123 1996; Remenda et al., 1996; Hansson et al., 2004). In the modeling community, a range of  
124 approaches have been applied to deal with frozen soil parameterizations. Earlier LSMs assumed  
125 no significant heat transfer and soil water redistribution for sub-freezing temperature, for example,  
126 in simplified SiB and BATS (Xue et al., 1991; Dickinson et al., 1993; Niu and Zeng, 2012). Koren  
127 et al. (1999) suggested that the frozen soil is permeable due to macropores that exist in soil  
128 structural aggregates, such as cracks, dead root passages, and worm holes. The NoahV3 model  
129 adopted this scheme as its default option. Niu and Yang (2006) suggested to separate a model grid  
130 into frozen and unfrozen patches, and these two patches have a linear effect on the soil hydraulic  
131 properties. This treatment was incorporated into CLM 3.0 and Noah-MP in 2007 and 2011,  
132 respectively.

Deleted: On the other hand, the s

Deleted: in cold region winters

Deleted: Previous field

Deleted: s

Deleted: there is a rich history in the

134 The spatial heterogeneity of soil moisture and WTD requires high-resolution meteorological input  
135 that direct outputs from GCMs are too coarse to provide. In GCMs, differences in simulated  
136 precipitation stem from the choice of convection parameterization scheme (Sherwood et al., 2014;

Deleted: Additionally, t

Deleted: Furthermore, i

Deleted: great uncertainties of

Deleted: s

153 Prein et al., 2015). An important approach to improve precipitation simulation is to conduct  
154 dynamical downscaling using the convection-permitting model (CPM) (Ban et al., 2014; Prein et  
155 al., 2015; Liu et al., 2017). The CPM uses a high spatial resolution (usually under 5-km) to  
156 explicitly resolve convection without activating convection parameterization schemes. CPMs can  
157 also improve the representation of fine-scale topography and spatial variations of surface fields  
158 (Prein et al., 2013). These CPM added-values provide an excellent opportunity to investigate water  
159 table dynamics in the PPR.

160  
161 The objectives of this paper are to 1) investigate the performance of a regional scale coupled land-  
162 groundwater model in simulating groundwater, water levels, recharge and storage in a seasonally  
163 frozen environment in PPR; and 2) explore the possible impacts of climate change on these  
164 processes.

165  
166 In this paper, we use a physical process-based LSM (Noah-MP) coupled with a groundwater  
167 dynamics model (MMF model). The coupled Noah-MP-MMF model is driven by two sets of  
168 meteorological forcing for 13 years under current and future climate scenarios. These two sets of  
169 meteorological dataset are from a CPM dynamical downscaling project using the Weather  
170 Research & Forecast (WRF) model with 4-km grid spacing covering the Contiguous U.S. and  
171 Southern Canada (WRF CONUS, Liu et al., 2017). The paper is structured as follows: Section 2  
172 introduces the groundwater observations for WTD evaluation in the PPR, the coupled Noah-MP-  
173 MMF model, and the meteorological forcing from the WRF CONUS project. Section 3 evaluates  
174 the model simulated WTD timeseries and shows the groundwater budget and hydrological changes  
175 due to climate change. Section 4 and 5 offer a broad discussion and conclusion.

Deleted: e

Deleted: recharge

Deleted: ,

Deleted: and evapotranspiration processes

Deleted: e

181 2. Data and Methods

182 2.1 Observational data

183 Groundwater observation data were obtained through several agencies: (1) the United States  
184 Geological Survey (USGS) National Water Information System in the U.S.  
185 (<https://waterdata.usgs.gov/nwis/gw>), (2) the Alberta Environment  
186 ([http://aep.alberta.ca/water/programs-and-services/groundwater/groundwater-observation-well-](http://aep.alberta.ca/water/programs-and-services/groundwater/groundwater-observation-well-network/default.aspx)  
187 [network/default.aspx](http://aep.alberta.ca/water/programs-and-services/groundwater/groundwater-observation-well-network/default.aspx)), (3) the Saskatchewan Water Security Agency  
188 (<https://www.wsask.ca/Water-Info/Ground-Water/Observation-Wells/>).

189

190 Initially, groundwater data from 160 wells were acquired, 72 in the U.S., 43 from Alberta, and 45  
191 from Saskatchewan. We used the following criteria to select qualified stations for our study and  
192 evaluate our model performance against these observations:

- 193 1) the location of the wells are within the PPR region;
- 194 2) a sufficiently long data record exists during the simulation period. We define the  
195 observation availability as the available observation period within the 13-year simulation  
196 period and select wells with observation availability greater than 80%;
- 197 3) we only take data from unconfined aquifers with shallow groundwater levels (mean WTD >  
198 5 m);
- 199 4) we only take data with minimal anthropogenic effects (such as from pumping or irrigation).

200  
201 These criteria reduced the observation data to 33 well records, with six in Alberta, 13 in  
202 Saskatchewan and 14 from the U.S. **Table 1** summarizes the information for each selected well,  
203 and **Fig. 1(a)** shows the location of the wells in our study area. It is noteworthy that most of the  
204 groundwater sites have more permeable deposits (sand and gravel) as provincial and state agencies

Deleted: close

Deleted: to

Deleted: -

Deleted: the record of

Deleted: 2

210 don't monitor low permeability formations. More information about the selecting criteria are  
211 provided in the supplemental materials.

212

213 **Fig. 1** (a) Topography of the Prairie Pothole Region (PPR) and station location of rain gauges (black dots) and  
214 groundwater wells (red diamonds); (b) Topography of the WRF CONUS domain, with the black box indicating the  
215 PPR domain.

216

217 **Table 1.** Summary of the locations and aquifer type and soil type of the 33 selected wells.

218

219

220 2.2 Groundwater and Frozen Soil Scheme in Noah-MP

221 In the present study, we used the community Noah-MP LSM (Niu et al. 2011; Yang et al. 2011),  
222 coupled with a GW model – the MMF model (Fan et al. 2007; Miguez-Macho et al., 2007). This  
223 coupled model has been applied in many regional hydrology studies in offline mode (Miguez-  
224 Macho and Fan 2012; Martinez et al., 2016) and coupled with regional climate models (Anyah et  
225 al., 2008; Barlage et al., 2015). We present here a brief introduction to the MMF groundwater  
226 scheme and the frozen soil scheme in Noah-MP, further details can be found in previous studies  
227 (Fan et al., 2007; Miguez-Macho et al., 2007; Niu and Yang, 2006).

228

229 Fig. 2 is a diagram of the structure of 4 soil layers (0.1, 0.3, 0.6 and 1.0 m) and the underlying  
230 unconfined aquifer in Noah-MP-MMF. The MMF scheme defines explicitly an unconfined aquifer  
231 below the 2-m soil and an auxiliary soil layer stretching to the WTD, which varies in space and  
232 time [m]. The thickness of this auxiliary layer ( $z_{aux}$  [m]) is also variable, depending on the WTD:

233 
$$z_{aux} = \begin{cases} 1, & WTD \geq -3 \\ -2 - WTD, & WTD < -3 \end{cases} \quad (1)$$

234

235 The vertical fluxes include gravity drainage and capillary flux, solved from the Richards' equation,

236 
$$q = K_{\theta} \left( \frac{\partial \psi}{\partial z} - 1 \right), \quad K_{\theta} = K_{sat} * \left( \frac{\theta}{\theta_{sat}} \right)^{2b+3}, \quad \psi = \psi_{sat} * \left( \frac{\theta_{sat}}{\theta} \right)^b \quad (2)$$

237 where  $q$  is water flux between two adjacent layers [m/s],  $K_{\theta}$  is the hydraulic conductivity [m/s] at

238 certain soil moisture content  $\theta$  [m<sup>3</sup>/m<sup>3</sup>],  $\psi$  is the soil **matric** potential [m] and  $b$  is soil pore size

239 index. The subscript *sat* denotes **saturation**. The recharge flux from/to the layer above WTD,  $R$ ,

240 can be obtained according to WTD:

Deleted: \*

Formatted: Centered

Deleted: (2)

Deleted: capillary

Deleted: saturated stateion. Therefore, tThe

$$R = \begin{cases} K_k * \left( \frac{\psi_i - \psi_k}{z_{soil(i)} - z_{soil(k)}} - 1 \right), & WTD \geq -2 \\ K_{aux} * \left( \frac{\psi_4 - \psi_{aux}}{(-2) - (-3)} - 1 \right), & -2 > WTD \geq -3 \\ K_{sat} * \left( \frac{\psi_{aux} - \psi_{sat}}{(-2) - (WTD)} - 1 \right), & WTD < -3 \end{cases} \quad (3)$$

246

247 In the first case, WTD is in the resolved soil layers and  $z_{soil}$  is the depth of soil layer with the  
 248 subscript  $k$  indicating the layer containing WTD while  $i$  is the layer above. The calculated water  
 249 table recharge is then passed to the MMF groundwater routine.

250

251 The change of groundwater storage in the unconfined aquifer considers three components:

252 recharge flux ( $R$ ), river discharge ( $Q_r$ ), and lateral flows ( $Q_{lat}$ ):

$$\Delta S_g = (R - Q_r + \sum Q_{lat}) \quad (4)$$

254 where  $S_g$  [mm] is groundwater storage,  $Q_r$  [mm] is the water flux of groundwater-river exchange,  
 255 and  $\sum Q_{lat}$  [mm] are groundwater lateral flows to/from all surrounding grid cells. The groundwater  
 256 lateral flow ( $\sum Q_{lat}$ ) is the total horizontal flows between each grid cell and its neighbouring grid  
 257 cells, calculated from Darcy's law with the Dupuit-Forchheimer approximation (Fan and Miguez-  
 258 Macho 2010), as:

$$Q_{lat} = wT \left( \frac{h - h_n}{l} \right) \quad (5)$$

260 where  $w$  is the width of cell interface [m],  $T$  is the transmissivity of groundwater flow [ $m^2/s$ ],  $h$   
 261 and  $h_n$  are the water table head [m] of local and neighboring cell, and  $l$  is the length [m] between  
 262 cells.  $T$  depends on hydraulic conductivity  $K$  and WTD:

Deleted:  $z_{k-1}$   
 Formatted: Font: Italic  
 Deleted:

Formatted: Font: Italic  
 Deleted: flux,  
 Deleted: ,

267  
268  
269  
270  
271  
272  
273  
274  
275  
276  
277  
278  
279  
280  
281  
282  
283  
284  
285  
286

$$T = \begin{cases} \int_{-\infty}^h K dz & WTD \geq -2 \\ \int_{-\infty}^{(z_{surf}-2)} K dz + \sum K_i * dz_i & WTD < -2 \end{cases} \quad (7)$$

For  $WTD < -2$ ,  $K$  is assumed to decay exponentially with depth,  $K = K_4 \exp(-z/f)$ ,  $K_4$  is the hydraulic conductivity in the 4-th soil layer and  $f$  is the e-folding length and depends on terrain slope. For  $WTD \geq -2$ ,  $i$  represents the number of layers between the water table and the 2-m bottom and  $z_{surf}$  is the surface elevation.

The river flux ( $Q_r$ ) is also represented by a Darcy's law-type equation, where the flux depends on the gradient between the groundwater and the river depth and the riverbed conductance:

$$Q_r = RC \cdot (h - z_{river}) \quad (8)$$

with  $z_{river}$  is the depth of river [m] and  $RC$  is dimensionless river conductance, which depends on the slope of the terrain and equilibrium water table. Eq. (8) is a simplification which uses  $z_{river}$  rather than the water level in the river and, for this study, we only consider one-way discharge from groundwater to rivers. Finally, the change of WTD is calculated as the total fluxes fill or drain the pore space between saturation and the equilibrium soil moisture state ( $\theta_{eq}$  [ $m^3/m^3$ ]) in the layer containing WTD:

$$\Delta WTD = \frac{\Delta S_g}{(\theta_{sat} - \theta_{eq})} \quad (9)$$

If  $\Delta S_g$  is greater than the pore space in the current layer, the soil moisture content of current layer is saturated and the WTD rises to the layer above, updating the soil moisture content in the layer above as well. Vice versa for negative  $\Delta S_g$  as water table declines and soil moisture decreases.

- Deleted:  $\leq$
- Deleted:  $\geq -2$
- Deleted:  $>$
- Deleted:  $< -2$

- Deleted:  $>$
- Deleted:  $WTD < -2$

- Deleted: which is
- Deleted: head, local
- Deleted: bed

- Deleted: bed
- Deleted: (eqzwt, [m]).
- Deleted: 7

299 **Fig. 2** Structure of the Noah-MP LSM coupled with MMF groundwater scheme, the top 2-m soil of 4 layers whose  
 300 thicknesses are 0.1, 0.3, 0.6 and 1.0 m. An unconfined aquifer is added below the 2-m boundary, including an auxiliary  
 301 layer and the saturated aquifer. Positive flux of  $R$  denotes downward transport. Two water table are shown, one within  
 302 the 2-m soil and one below, indicating that the model is capable to deal with both shallow and deep water table.

303  
 304 There are two options in Noah-MP LSM for frozen soil permeability; option 1, the default option  
 305 in Noah-MP, is from Niu and Yang (2006) and option 2 is inherited the Koren et al. (1999) scheme  
 306 from NoahV3. Option 1 assumes that a model grid cell consists of permeable and impermeable  
 307 patches and the area weighted sum of these patches gives the grid cell soil hydraulic properties.

308 Thus, the total soil moisture ( $\theta$ ) in the grid cell is used to compute hydraulic properties as:

$$\theta = \theta_{ice} + \theta_{liq} \quad (10)$$

$$K = (1 - F_{frz})K_u = (1 - F_{frz})K_{sat} \left( \frac{\theta}{\theta_{sat}} \right)^{2b+3} \quad (11)$$

311 the subscript  $fz$  and  $u$  denote the frozen and unfrozen patches in the grid point. The impermeable  
 312 frozen soil fraction is parameterized as:

$$F_{frz} = e^{-\alpha(1-\theta_{ice}/\theta_{sat})} - e^{-\alpha} \quad (12)$$

314  $\alpha = 3.0$  is an adjustable parameter. The amount of the liquid water in soil layer is either  $\theta_{liq}$  or  
 315  $\theta_{liq,max}$ , the maximum amount of liquid water, which is calculated by a more general form of the  
 316 freezing-point depression equation:

$$\theta_{liq,max} = \theta_{sat} \left\{ \frac{10^3 L_f (T_{soil} - T_{frz})}{\theta T_{soil} \psi_{sat}} \right\}^{\frac{1}{b}} \quad (13)$$

318 where  $T_{soil}$  and  $T_{frz}$  are soil temperature and freezing point [K];  $L_f$  is the latent heat of fusion [J  
 319  $kg^{-1}$ ];  $g$  is gravitational acceleration [ $m s^{-2}$ ].

320

Formatted: Font: 12 pt

Deleted: integrate a linear effect on

Formatted ... [1]

Formatted ... [2]

Deleted:  $\psi = \psi_u = \psi_{sat} \left( \frac{\theta}{\theta_{sat}} \right)^{-b}$

Formatted ... [3]

Deleted: t

Formatted ... [4]

Formatted ... [5]

Formatted ... [6]

Formatted ... [7]

Formatted ... [8]

Formatted ... [9]

Formatted ... [10]

Formatted ... [12]

Deleted: ¶

Formatted ... [11]



329 On the other hand, the option 2 uses only the liquid water volume to calculate hydraulic properties  
330 and assumes a non-linear effect of frozen soil on permeability. Also, the option 2 uses a variant of  
331 freezing-point depression equation with an extra term,  $(1 + 8\theta_{ice})^2$ , to account for the increased  
332 interface between soil particles and liquid water due to the increase of ice crystals. Generally,  
333 option 1 assumes that soil ice has a smaller effect on infiltration and simulates more permeable  
334 frozen soil than option 2 (Niu et al., 2011). For this reason, the option 1 allows the soil water to  
335 move and redistribute more easily within the frozen soil and we decide to use option 1 in our study.

Deleted: However

Formatted: Font: 12 pt

Formatted: Font: 12 pt

Formatted: Font: 12 pt

Formatted: Font: 12 pt

Formatted: Font: 12 pt

337 2.3 Forcing Data

338 The output from the WRF CONUS dataset (Liu et al. 2017) are used as meteorological forcing to  
339 drive the Noah-MP-MMF model. The WRF CONUS project consists of two simulations. The first  
340 simulation is referred as the current climate scenario, or control run (CTRL), from Oct 2000 to Sep  
341 2013, and forced with the 6-hourly 0.7° ERA-Interim reanalysis data. The second simulation is a  
342 perturbation to reflect the future climate scenario, closely following the pseudo global warming  
343 (PGW) approach in previous works (Rasmussen et al., 2014). The PGW simulation is forced with  
344 6-hourly ERA-Interim reanalysis data plus a delta climate change signal derived from an ensemble  
345 of CMIP5 models under the RCP8.5 emission scenario and reflects the climate change signal  
346 between the end of 21<sup>st</sup> and 20<sup>th</sup> century.

347

348 **Fig. 3** shows the annual precipitation in the PPR from 4-km WRF CONUS from the current climate  
349 and 32-km North America Regional Reanalysis (NARR, another reanalysis dataset commonly  
350 used for land surface model forcing). Both datasets show similar annual precipitation pattern and  
351 bias patterns compared to observations: underestimating of precipitation in the east and  
352 overestimating in the west. However, the WRF CONUS shows significant improvement of  
353 percentage bias in precipitation  $((\text{Model-Observation})/\text{Observation})$  over the western PPR. For the  
354 consistency of the same source of data for current and future climate, the WRF-CONUS is the best  
355 available dataset for the coupled land-groundwater study in the PPR.

356

357 **Fig. 3** Evaluation of the annual precipitation from WRF CONUS (top) and NARR (bottom) against rain gauge  
358 observation.

359

360 For the future climate study, the precipitation and temperature of the PGW climate forcing are  
361 shown in **Fig. 4** and **Fig. 5**. The WRF CONUS projects more precipitation in the PPR, except in  
362 the southeast of the domain in summer, where it shows a precipitation reduction of about 50 to 100  
363 mm. On the other hand, the WRF CONUS projects strongest warming occurring in the northeast  
364 PPR in winter (**Fig. 5**), about 6–8 °C. Another significant warming signal occurs in summer in the  
365 southeast of domain, corresponding to the reduction of future precipitation, as seen in **Fig. 4**.

366

367 **Fig. 4** Seasonal accumulated precipitation from current climate scenario(CTRL), future climate scenario (PGW) and  
368 projected change (PGW-CTRL) in the forcing data.

369

370 **Fig. 5** Seasonal averaged temperature from CTRL, PGW, and the projected change (PGW-CTRL).

371

372 2.4 Model Setup

373 The two Noah-MP-MMF simulations representing the current climate and future climate are  
374 denoted as CTRL and PGW, respectively. The initial groundwater levels are from a global 1-km  
375 equilibrium groundwater map (Fan et al., 2013) and the equilibrium soil moisture for each soil  
376 layer is calculated at the first model timestep with climatology recharge, spinning up for 500 years.  
377 Since the model domain is at a different resolution than the input data, the appropriate initial WTD  
378 at 4-km may be different than the average at 1-km. To properly initialize the simulation, we spin  
379 up the model using the forcing of current climate (CTRL) for the years from 2000 to 2001  
380 repeatedly (in total 10 loops).

381

382 Due to different data sources, the default soil types along the boundary between the U.S. and  
383 Canada are discontinuous. Thus, we use the global 1-km fine soil data (Shangguan et al., 2014,  
384 <http://globalchange.bnu.edu.cn/research/soilw>) in our study region. The soil properties for the  
385 aquifer use the same properties as the lowest soil layer from the Noah-MP 2-m soil layers.

386 3. Results

387 3.1 Comparison with groundwater observations

388 According to the locations of 33 groundwater wells in **Table 1**, the simulated WTD from the  
389 closest model grid points are extracted. **Fig. 6** shows the modeled WTD bias from the CTRL run.  
390 We also select the monthly WTD timeseries from 8 sites, the observation are in black dots and  
391 CTRL in blue lines. See supplemental materials for the timeseries of 33 sites. The model produces  
392 reasonable values of mean WTD, the mean bias are smaller than 1 m in most of sites, except in  
393 Alberta, where the model predicts deep bias **about 5 m in the northwestern part of PPR**. The model  
394 also successfully captures the annual cycle of WTD, which rises in spring and early summer,  
395 because of snowmelt and rainfall recharge, and declines in summer and fall, because of high ET,  
396 and in winter because of frozen near-surface soil. In all observations, the timing of **the** water table  
397 rising and dropping is well simulated, as the timing and amount of infiltration and recharge in  
398 spring is controlled by the freeze-thaw processes in seasonally frozen soil.

399

400 **Fig. 6.** WTD (m) bias from CTRL simulation and timeseries from 8 groundwater wells in PPR (black for observation and  
401 blue for CTRL model simulation). See Table 2 CTRL column for the model statistics and supplemental materials for complete  
402 timeseries from 33 wells.

404 On the other hand, the model simulated WTD seasonal variation is smaller than observations. The  
405 small seasonal variation could be due to the misrepresentation between the lithology from the  
406 observational surveys and the soil types in the model grids. As mentioned in Section 2.2, the  
407 groundwater aquifer uses the same soil types as the bottom layer of the resolved 2-m soil layers.  
408 While sand and gravel are the dominant lithology in most of the sites, they are mostly clay and  
409 loam in the model (Table 1). For sandy soil reported in most of the sites, small capacity and fast  
410 responses to infiltration lead to large water table fluctuations, whereas, in the model, clay and loam

Deleted: mountainous region

Deleted: **Fig. 6.** WTD (m) bias from CTRL simulation and timeseries from 8 groundwater wells in PPR. See Table 2 CTRL column for the model statistics and supplemental materials for complete timeseries from 33 wells.

Formatted: Right: -1.49 cm

Formatted: Font: Times, 10 pt

416 soil allows low permeability and large capacity, and smoothens responses to recharge and capillary  
417 effects. Furthermore, the 4-layer soils are vertically homogeneous in soil type and the groundwater  
418 model uses the lowest level soil type as the aquifer lithology. For many part of the PPR, where  
419 groundwater level are perched at the top 5-m due to a layer called glacial till. These,  
420 geohydrological characteristics cannot be reflected in this model and contribute to the deep WTD  
421 bias simulated in Alberta. This shortcoming of the model was also reported in a study taken place  
422 in the Amazon rainforest (Miguez-Macho et al., 2012).

423

Deleted: is

425 3.2 Climate change signal in Groundwater fluxes

426 The MMF groundwater model simulates three components in the groundwater water budget, the  
427 recharge flux ( $R$ ), lateral flow ( $Q_{lat}$ ), and discharge flux to rivers ( $Q_r$ ). Because the topography is  
428 usually flat in the PPR, the magnitude of groundwater lateral transport is very small ( $Q_{lat}$  less than  
429 5 mm per year). On the other hand, the shallow water table in the PPR region is higher than the  
430 local river bed, thus, the  $Q_r$  term is always discharging from groundwater aquifers to rivers. As a  
431 result, the recharge term is the major contributor to the groundwater storage in the PPR, and its  
432 variation (usually between -100 to 100 mm) dominates the timing and amplitude of the water table  
433 dynamics. The seasonal accumulated total groundwater fluxes in the PPR ( $R+Q_{lat} - Q_r$ ) are  
434 shown in **Fig. 7**. The positive (negative) flux in blue (red) means the groundwater aquifer is gaining  
435 (losing) water, causing the water table to rise, (decline).

436

437 **Fig. 7** Seasonal accumulated total groundwater fluxes ( $R+$  ) for current climate (CTRL, top), future climate (PGW,  
438 middle) and projected change (PGW-CTRL, bottom) in forcing data. Black dashed lines in PGW-CTRL separate the  
439 PPR into eastern and western halves.  
440

441 Under current climate conditions, the total groundwater fluxes show strong seasonal fluctuations,  
442 consistent with the WTD timeseries shown in **Fig. 6**. On average, in fall (SON) and winter (DJF),  
443 there is a 20-mm negative recharge, driven by the capillary effects and drawing water from aquifer  
444 to dry soil above. Spring (MAM) is usually the season with a strong positive recharge because  
445 snowmelt provides a significant amount of water, and soils thawing allow infiltration. The large  
446 amount of snowmelt water contributes to more than 100 mm of positive recharge in the eastern  
447 domain. It is until summer (JJA), when strong ET depletes soil moisture and results in about 50  
448 mm of negative recharge.

449

Deleted: s

451 Under future climate conditions, the increased PR in fall and winter leads to wetter upper soil  
452 layers, resulting in a net positive recharge flux (PGW – CTRL in SON and DJF). However, the  
453 PGW summer is impacted by increased ET under a warmer and drier climate, due to higher  
454 temperature and less PR. As a result, the groundwater uptake by the capillary effect is more critical  
455 in the future summer. Furthermore, there is a strong east-to-west difference in the total  
456 groundwater flux change from PGW to CTRL. In the eastern PPR, the change in total groundwater  
457 flux exhibits obvious seasonality while the model projects persistent positive groundwater fluxes  
458 in the western PPR.

459



460 3.3 Water budget analysis

461 **Fig. 8** and **Fig. 9** show the water budget analysis for the eastern and western PPR (divided by the  
462 dotted line in 103° W in Fig. 7), respectively. Four components are presented in the figures, i.e.  
463 (1) PR and ET; (2) surface and underground runoff (*SFCRUN* and *UDGRUN*); and surface  
464 snowpack; (3) the change of soil moisture storage and (4) groundwater fluxes and the change of  
465 storage. In **the** current and future climate, these budget terms are plotted in annual accumulation  
466 ((a) and (b) for CTRL and PGW), whereas their difference are plotted in each month individually  
467 ((c) for PGW-CTRL).

468

469 Under current climate conditions, during snowmelt infiltration and rainfall events, water infiltrates  
470 into the top soil layer, travels through the soil column and exits the bottom of the 2-m boundary,  
471 hence, the water table rises. During the summer dry season, ET is higher than PR and the soil  
472 layers lose water through ET, therefore, the capillary effect takes water from the underlying aquifer  
473 and the water table declines. In winter, the near-surface soil in the PPR is seasonally frozen, thus,  
474 a redistribution of subsurface water to the freezing front results in negative recharge, and the water  
475 table declines.

476

477 In the eastern PPR, the effective precipitation (PR-ET) is found to increase from fall to spring, but  
478 decrease in summer in PGW (**Fig. 8(1c)**). Warmer falls and winters in PGW, together with  
479 increased PR, not only delay snow accumulation and bring forward snowmelt, but also change  
480 the precipitation partition – more as rain and less as snow. This warming causes up to 20 mm of  
481 snowpack loss (**Fig.8(2c)**). The underground runoff starts much earlier in PGW (December)  
482 (**Fig.8(2b)**) than in CTRL (February) (**Fig.8(2a)**). On the other hand, the warming in PGW also

483 changes the partitioning of soil ice and soil water in subsurface soil layers (**Fig. 8(3c)**). For late  
484 spring in PGW, the springtime recharge in the future is significantly reduced due to early melting  
485 and less snowpack remaining (**Fig. 8(4c)**). In the PGW summer, reduced PR (50 mm less) and  
486 higher temperatures (8 °C warmer) lead to reduction in total soil moisture, and a stronger negative  
487 recharge from the aquifer. Therefore, the increase of recharge from fall to early spring compensates  
488 the recharge reduction due to stronger ET in summer in the eastern PPR, and changes little in the  
489 annual mean groundwater storage (1.763 mm per year).

490

491 **Fig. 8** Water budget analysis in the eastern PPR in (a) CTRL, (b) PGW and (c) PGW – CTRL. Water budget terms  
492 include: (1) *PR* & *ET*, (2) surface snow, surface runoff and underground runoff (*SNOW*, *SFCRUN*, and *UDGRUN*),  
493 (3) change of soil moisture storage (soil water, soil ice and total soil moisture,  $\Delta S_{MC}$ ) and (4) groundwater fluxes  
494 and the change of groundwater storage ( $R$ ,  $Q_{lat}$ ,  $Q_r$ ,  $\Delta S_g$ ). The annual mean soil moisture change (PGW-CTRL) is  
495 shown with black dashed line in (3). The Residual term is defined as  $Res = (R+Q_{lat}-Q_r)-\Delta S_g$  in (4). Note that in (a)  
496 and (b) the accumulated fluxes and change in storage are shown in lines, whereas in (c) the difference in (PGW-CTRL)  
497 is shown for each individual month in bars.

498

499 These changes in water budget components in the western PPR (**Fig. 9**) are similar to those in the  
500 eastern PPR (**Fig. 8**), except in summer. The reduction in summer PR in the western the PPR (less  
501 than 5 mm reduction) is not as obvious as that in the eastern PPR (50 mm reduction) (**Fig. 4**). Thus,  
502 annual mean total soil moisture in future is about the same as in current climate (Fig. 9(3c)) and  
503 results in little negative recharge in PGW summer (**Fig. 9(4c)**). Therefore, the increase in annual  
504 recharge is more significant (10 mm per year), an increase of about 50% of the annual recharge in  
505 the current climate (20 mm per year) (**Fig. 9(4c)**).

506

507 **Fig. 9** Same as Fig. 8. Water budget analysis in the western PPR: in (a) CTRL, (b) PGW and (c) PGW – CTRL.  
508 Water budget terms include: (1) *PR & ET*, (2) surface snow, surface runoff and underground runoff (*SNOW, SFCRUN,*  
509 *and UDGRUN*), (3) change of soil moisture storage (soil water, soil ice and total soil moisture,  $\Delta SMC$ ) and (4)  
510 groundwater fluxes and the change of groundwater storage ( $R, Q_{lat}, Q_r, \Delta S_g$ ). The annual mean soil moisture change  
511 (PGW-CTRL) is shown with black dashed line in (3). The Residual term is defined as  $Res = (R + Q_{lat} - Q_r) - \Delta S_g$  in (4).  
512 Note that in (a) and (b) the accumulated fluxes and change in storage are shown in lines, whereas in (c) the difference  
513 in (PGW-CTRL) is shown for each individual month in bars.  
514

Deleted: Fig. 9 Same as Fig. 8, but for the western PPR. ¶

515 In both the eastern and western PPR, the water budget components for the groundwater aquifer are  
516 plotted in **Fig. 8(4)** and **Fig. 9 (4)**, with the changes of each flux (PGW-CTRL) printed at the  
517 bottom. The groundwater lateral flow is a small term in areal average and has little impact on the  
518 groundwater storage. Nearly half of the increased recharge in both the eastern and western PPR is  
519 discharged to river flux ( $Q_r = 2.26$  mm out of  $R = 4.15$  mm in the eastern PPR and  $Q_r = 5.20$  mm  
520 out of  $R = 10.72$  mm in western PPR). Therefore, the groundwater storage change in the eastern  
521 PPR (1.76 mm per year) is not as great as that in the western PPR (5.39 mm per year).

522

523 These two regions of the PPR show differences in hydrological response to future climate because  
524 of the spatial variation of the summer PR. As shown in both **Fig. 4** (PGW-CTRL), **Fig. 8(1)** and  
525 **Fig. 9(1)**, the reduction of future PR in summer in the eastern PPR is significant (50 mm). The  
526 spatial difference of precipitation changes in the PPR further results in the recharge increase  
527 doubling in the western PPR compared to the eastern PPR.

528

530 4. Discussion

531 4.1 Improving WTD Simulation

532 In Section 3.1, we show that the model is capable of simulating the mean WTD in most sites, yet  
533 predicts deep groundwater in Alberta and underestimates its seasonal variation. These results may  
534 be due to misrepresentations between model default soil type and the soil properties in the  
535 observational wells. To test this theory, an additional simulation, REP, is conducted by replacing  
536 the default soil types in the locations of these 33 groundwater wells with sand-type soil, which is  
537 the dominant soil types reported from observational surveys. The timeseries of the REP and default  
538 CTRL are shown in Fig. 10 (also see supplemental materials for the complete 33 sites) and a  
539 summary of the mean and standard deviation of the two simulations are provided in Table 2.

540

541 Fig. 10 Same as Fig. 6. WTD (m) bias from CTRL simulation and timeseries from 8 groundwater wells in PPR (black for  
542 observation and blue for CTRL model simulation, and red for the replacing soil type simulation). REP is the additional  
543 simulation by replacing the default soil type in the model with sandy soil type.

545 The REP simulation with sandy soil show two sensitive signals: (1) REP WTD are shallower than  
546 the default simulation; (2) and exhibit stronger seasonal variation. These two signals can be  
547 explained by the WTD equation in the MMF scheme:

548 
$$\Delta WTD = \frac{\Delta(R + Q_{lat} - Q_r)}{(\theta_{sat} - \theta_{eq})} \quad (14)$$

549 Eq. (14) represents that the change of WTD in a period of time is calculated by the total  
550 groundwater fluxes,  $\Delta(R + Q_{lat} - Q_r)$ , divided by the available soil moisture capacity of current  
551 layer  $(\theta_{sat} - \theta_{eq})$ . In REP simulation, the parameters  $\theta_{sat}$  for the dominant soil type in  
552 observational sites (sand/gravel) is smaller than those in default model grids (clay loam, sandy  
553 loam, loam, loamy sand, etc.). Therefore, changing the  $\theta_{sat}$  is essentially reducing the storage in

Deleted: Fig. 10 Same as Fig. 6, the timeseries of simulated WTD from both default model (blue) and replacing soil type simulation, REP (red). REP is the additional simulation by replacing the default soil type in the model with sandy soil type

Formatted: Right: -1.49 cm

Formatted: Font: 10 pt

Deleted: 0

Deleted: 0

560 the aquifer and soil in this model grid. Given the same amount of groundwater flux, in the REP  
561 simulation, the mean WTD is higher and the seasonal variation is stronger than the default CTRL  
562 run.

563

564 In the REP simulation, we replaced soil type only at a limited number of sites because the  
565 geological survey data in high resolution and large area extent is not yet available for the whole  
566 PPR. At point scale, the WTD responses to climate change over these limited number of sites show  
567 diverse results and uncertainties (see supplemental materials). For the rest of the domain, the  
568 default soil type from global 1-km soil map is used. The REP modifications of soil types at point-  
569 scale have small contribution to the water balance analysis (Fig. 8 & 9) at regional-scale. Our  
570 results and conclusions for groundwater response to PGW doesn't change. We are currently  
571 undertaking a soil property survey project in the PPR region to obtain soil properties at high spatial  
572 resolution, both horizontal and vertical. This may provide better opportunity to improve WTD  
573 simulation as well as assess climate-groundwater interaction in future studies.

574

#### 575 4.2 Climate Change Impacts on Groundwater Hydrological Regime

576 The warming and increased precipitation in cold seasons in future climate lead to later snow  
577 accumulation, higher recharge in winter and earlier melting in spring compared to current climate.

578 Such changes in snowpack loss have been hypothesized in mountainous as well as high-latitude  
579 regions (Taylor et al 2013; Ireson et al., 2015; Meixner et al., 2016; Musselman et al., 2017). In  
580 addition to the amount of recharge, the shift of recharge season is also noteworthy. Under current  
581 climate conditions in spring, soil thawing (in March) is generally later than snowmelt (in February)  
582 by a month in the PPR. Thus, the snowmelt water in pre-thaw spring would either re-freeze after

Deleted: c

Deleted: Climate change induced warming in high-latitudes winter and increased precipitation, including a higher liquid fraction, in PGW winter results in later snow accumulation, higher winter recharge and earlier melting in spring.

Deleted: ¶

590 infiltrating into partially frozen soil or become surface runoff. Under the PGW climate, the warmer  
591 winter and spring allows snowmelt and soil thaw to occur earlier in the middle of winter (in January  
592 and February, respectively). As a result, the recharge season starts earlier in December, and last  
593 longer until June, results in longer recharge season but with lower recharge rate.

594

595 Future projected increasing evapotranspiration demand in summer desiccates soil moisture,  
596 resulting in more water uptake from aquifers to subsidize dry soil in the future summer. This  
597 groundwater transport to soil moisture is similar to the “buffer effect” documented in an offline  
598 study in the Amazon rainforest (Pokhrel et al., 2014). In , shallow water tables exist in the critical  
599 zone, where WTD ranges from 1 to 5 meters below surface and could exert strong influence on  
600 land energy and moisture fluxes feedback to the atmosphere (Kollet and Maxwell, 2008; Fan ,  
601 2015). Previous coupled atmosphere-land-groundwater studies at 30-km resolution showed that  
602 groundwater could support soil moisture during summer dry period, but has little impacts on  
603 precipitation in Central U.S. (Barlage et al., 2015). It would be an interesting topic to study the  
604 integrated impacts of shallow groundwater to regional climate in the convection permitting  
605 resolution (resolution < 5-km).

606

#### 607 4.3 Fine-scale interaction between groundwater and Prairie pothole wetlands

608 Furthermore, groundwater exchange with prairie pothole wetlands are complicated and critical in  
609 the PPR. Numerous wetlands known as potholes or sloughs provide important ecosystem services,  
610 such as providing wildlife habitats and groundwater recharge (Johnson et al., 2010). Shallow  
611 groundwater aquifers may receive water from or lose water to prairie wetlands depending on the  
612 hydrological setting. Depression-focused recharge generated by runoff from upland to depression

613 contributes to sufficient amount of water input to shallow groundwater (5-40 mm/year) (Hayashi  
614 et al., 2016).

615

616 On the other hand, groundwater lateral flow exchange center of a wetland pond to its moist margin

617 is also an important component in the wetland water balance (van der Kamp and Hayashi, 2009;

618 Brannen, et al., 2015; Hayashi et al., 2016). However, this groundwater-wetland exchange

619 typically occurs on local scale (from 10 to 100 m) and thus, is challenging to represent in current

620 land surface models or climate models (resolution from 1 km to 100 km). In this paper, we focus

621 on the groundwater dynamics on regional scale, which is still unable to capture these small wetland

622 features in this study. We admit this limitation and are currently developing a sub-grid scheme to

623 represent small scale open water wetlands as a fraction within a grid cell and calculate its feedback

624 to regional environments. Future studies on this topic will provide valuable insights on these key

625 ecosystems and their interaction under climate change.

626

Deleted: s

Deleted: therefore,

Deleted: our model

Deleted: challenge

631 Conclusion

632 In this study, a coupled land-groundwater model is applied to simulate the interaction between the  
633 groundwater aquifer and soil moisture in the PPR. The climate forcing is from a dynamical  
634 downscaling project (WRF CONUS), which uses the convection-permitting model (CPM)  
635 configuration in high resolution. The goal of this study is to investigate the groundwater responses  
636 to climate change, and to identify the major processes that contribute to these responses in the PPR.

637 To our knowledge, this is the first study applying CPM forcing in a hydrology study in this region.

638 We have three main findings:

639

640 (1) the coupled land-groundwater model shows reliable simulation of mean WTD, however  
641 underestimates the seasonal variation of the water table against well observations. This could be  
642 attributed to several reasons, including misrepresentation of topography and soil types, as well as  
643 vertical homogenous soil layers used in the model. We further conducted an additional simulation  
644 (REP) by replacing the model default soil types with sand-type soil and the simulated WTDs were  
645 improved in both mean and seasonal variation. However, inadequacy of soil properties in deeper  
646 layer and higher spatial resolution is still a limitation.

647

648 (2) Recharge markedly increases due to projected increased PR, particularly from fall to spring  
649 under future climate conditions. Strong east-west spatial variation exists in the annual recharge  
650 increases, 25% in the eastern and 50% in the western PPR. This is due to the significant projected  
651 PR reduction in PGW summer in the eastern PPR but little change in the western PPR. This PR  
652 reduction leads to stronger ET demand, which draws more groundwater uptake due to the capillary  
653 effect, results in negative recharge in the summer. Therefore, the increased recharge from fall to



654 spring is consumed by ET in summer, and results in little change in groundwater in the eastern  
655 PPR, while gaining water in the western PPR.

656

657 (3) The timing of infiltration and recharge are critically impacted by the changes in freeze-thaw  
658 processes. Increased precipitation, combined with higher winter temperatures, results in later snow  
659 accumulation/soil freezing, partitioned more as rain than snow, and earlier snowmelt/soil thaw.  
660 This leads to substantial loss of snowpack, shorter frozen soil season, and higher permeability in  
661 soil allowing infiltration. Late accumulation/freezing and early melting/thawing leads to an early  
662 start of a longer recharge season from December to June, but with a lower recharge rate.

663

664 Our study has some limitations where future studies are encouraged:

665 (1) Despite the large number of groundwater wells in PPR, only a few are suitable for long-term  
666 evaluation, due to data quality, anthropogenic pumping, and length of data record. As remote  
667 sensing techniques advance, observing terrestrial water storage anomalies derived from the  
668 GRACE satellite may provide substantial information on WTD, although the GRACE information  
669 needs to be downscaled to a finer scale before comparisons can be made with regional hydrology  
670 models at km-scale (Pokhrel et al., 2013).

671

672 (2) This study is an offline study of climate change impacts on groundwater. It is important to  
673 investigate how shallow groundwater in the earth's critical zone could interact with surface water  
674 and energy exchange to the atmosphere and affect regional climate. This investigation would be  
675 important to the central North America region (one of the land atmosphere coupling "hot spots",  
676 Koster et al., 2004 ).

677

678 **Acknowledgments**

679 The authors Zhe Zhang, Yanping Li, Zhenhua Li gratefully acknowledge the support from the  
680 Changing Cold Regions Network (CCRN) funded by the Natural Science and Engineering  
681 Research Council of Canada (NSERC), as well as the Global Water Future project and Global  
682 Institute of Water Security at University of Saskatchewan. Yanping Li acknowledge the support  
683 from NSERC Discovery Grant. Fei Chen, Michael Barlage appreciate the support from the Water  
684 System Program at the National Center for Atmospheric Research (NCAR), USDA NIFA Grants  
685 2015-67003-23508 and 2015-67003-23460, NSF INFEW/T2 Grant #1739705, and NOAA CFDA  
686 Grant #NA18OAR4590381. NCAR is sponsored by the National Science Foundation. Any  
687 opinions, findings, conclusions or recommendations expressed in this publication are those of the  
688 authors and do not necessarily reflect the views of the National Science Foundation.

689

690 Reference

- 691 Anyah, R. O., Weaver, C. P., Miguez-macho, G., Fan, Y. and Robock, A.: Incorporating water  
692 table dynamics in climate modeling : 3 . Simulated groundwater influence on coupled land-  
693 atmosphere variability, , 113, 1–15, doi:10.1029/2007JD009087, 2008.
- 694 Ban, N., Schmidli, J. and Schär, C.: Evaluation of the new convective-resolving regional climate  
695 modeling approach in decade-long simulations, *J. Geophys. Res. Atmos.*, 119, 7889–7907,  
696 doi:10.1002/2014JD021478.Received, 2014.
- 697 Barlage, M., Tewari, M., Chen, F., Miguez-Macho, G., Yang, Z. L. and Niu, G. Y.: The effect of  
698 groundwater interaction in North American regional climate simulations with WRF/Noah-MP,  
699 *Clim. Change*, 129(3–4), 485–498, doi:10.1007/s10584-014-1308-8, 2015.
- 700 Brannen, R., Spence, C. and Ireson, A.: Influence of shallow groundwater-surface water  
701 interactions on the hydrological connectivity and water budget of a wetland complex, *Hydrol.*  
702 *Process.*, 29(18), 3862–3877, doi:10.1002/hyp.10563, 2015.
- 703 Christensen NS, Wood AW, Voisin N, et al (2004) The Effects of Climate Change on the  
704 Hydrology and Water Resources of the Colorado River Basin. *Clim Change* 62:337–363. doi:  
705 10.1023/B:CLIM.0000013684.13621.1f
- 706 Dickinson RE, Henderson-Sellers A, Kennedy PJ (1993) Biosphere-Atmosphere Transfer Scheme  
707 (BATS) Version 1e as Coupled to the NCAR Community Climate Model. NCAR Technical  
708 Note, NCAR/TN-387+STR.
- 709 Döll, P. and Fiedler, K.: Global-scale modeling of groundwater recharge, *Hydrol. Earth Syst. Sci.*,  
710 12(3), 863–885, doi:10.5194/hess-12-863-2008, 2008.
- 711 Döll, P.: Vulnerability to the impact of climate change on renewable groundwater resources: A  
712 global-scale assessment, *Environ. Res. Lett.*, 4(3), doi:10.1088/1748-9326/4/3/035006, 2009.
- 713 Dumanski, S., Pomeroy, J. W. and Westbrook, C. J.: Hydrological regime changes in a Canadian  
714 Prairie basin, *Hydrol. Process.*, 29(18), 3893–3904, doi:10.1002/hyp.10567, 2015.
- 715 Environment Canada: Municipal Water Use, 2009 Statistics, 2011 Munic. Water Use Rep., 24,  
716 doi:En11-2/2009E-PDF Information, 2011.
- 717 Fan Y, Miguez-Macho G, Weaver CP, et al (2007) Incorporating water table dynamics in climate  
718 modeling: 1. Water table observations and equilibrium water table simulations. *J Geophys*  
719 *Res Atmos* 112:1–17. doi: 10.1029/2006JD008111
- 720 Fan, Y., Li, H. and Miguez-Macho, G.: Global patterns of groundwater table depth, *Science* (80-. ),  
721 339(6122), 940–943, doi:10.1126/science.1229881, 2013.
- 722 Fan, Y.: Groundwater in the Earth’s critical zones: Relevance to large-scale patterns and processes,  
723 *Water Resour. Res.*, 3052–3069, doi:10.1002/2015WR017037.Received, 2015.
- 724 Granger RJ, Gray DM: Evaporation from natural non-saturated surface. *J. Hydrol.*, 111, 21–29,  
725 1989.
- 726 Gray DM: Handbook on the Principles of Hydrology: With Special Emphasis Directed to Canadian  
727 Conditions in the Discussion, Applications, and Presentation of Data. Water Information  
728 Center: Huntingdon, New York, 1970. ISBN:0-912394-07-2
- 729 Green, T. R., Taniguchi, M., Kooi, H., Gurdak, J. J., Allen, D. M., Hiscock, K. M., Treidel, H. and  
730 Aureli, A.: Beneath the surface of global change: Impacts of climate change on groundwater,  
731 *J. Hydrol.*, 405(3–4), 532–560, doi:10.1016/j.jhydrol.2011.05.002, 2011.
- 732 Hayashi, M., Van Der Kamp, G. and Schmidt, R.: Focused infiltration of snowmelt water in  
733 partially frozen soil under small depressions, *J. Hydrol.*, 270(3–4), 214–229,  
734 doi:10.1016/S0022-1694(02)00287-1, 2003.

735 Hayashi, M., van der Kamp, G. and Rosenberry, D. O.: Hydrology of Prairie Wetlands:  
736 Understanding the Integrated Surface-Water and Groundwater Processes, *Wetlands*, 36, 237–  
737 254, doi:10.1007/s13157-016-0797-9, 2016.

738 Ireson, A. M., van der Kamp, G., Ferguson, G., Nachshon, U. and Wheater, H. S.: Hydrogeological  
739 processes in seasonally frozen northern latitudes: understanding, gaps and challenges,  
740 *Hydrogeol. J.*, 21(1), 53–66, doi:10.1007/s10040-012-0916-5, 2013.

741 Ireson, A. M., Barr, A. G., Johnstone, J. F., Mamet, S. D., van der Kamp, G., Whitfield, C. J.,  
742 Michel, N. L., North, R. L., Westbrook, C. J., DeBeer, C., Chun, K. P., Nazemi, A. and Sagin,  
743 J.: The changing water cycle: the Boreal Plains ecozone of Western Canada, *Wiley Interdiscip.*  
744 *Rev. Water*, 2(5), 505–521, doi:10.1002/wat2.1098, 2015.

745 Johnson, W. C., Werner, B., Guntenspergen, G. R., Voldseth, R. A., Millett, B., Naugle, D. E.,  
746 Tulbure, M., Carroll, R. W. H., Tracy, J. and Olawsky, C.: Prairie Wetland Complexes as  
747 Landscape Functional Units in a Changing Climate, *Bioscience*, 60(2), 128–140,  
748 doi:10.1525/bio.2010.60.2.7, 2010.

749 Kelln C, Barbour L, Qualizza C (2007) Preferential Flow in a Reclamation Cover : Hydrological  
750 and Geochemical Response. 1277–1289

751 Koren, V., Schaake, J., Mitchell, K., Duan, Q.-Y., Chen, F., & Baker, J. M. (1999). A  
752 parameterization of snowpack and frozen ground intended for NCEP weather and climate  
753 models. *Journal of Geophysical Research: Atmospheres*, 104(D16), 19569–19585.  
754 <https://doi.org/10.1029/1999JD900232>

755 Koster, R. D., Dirmeyer, P. A., Guo, Z., Bonan, G., Chan, E., Cox, P., Gordon, C. T., Kanae, S.,  
756 Kowalczyk, E., Lawrence, D., Liu, P., Lu, C.-H., Malyshev, S., McAvaney, B., Mitchell,  
757 K., Mocko, D., Oki, T., Oleson, K., Pitman, A., Sud, Y. C., Taylor, C. M., Verseghy, D.,  
758 Vasic, R., Xue, Y. and Yamada, T.: Regions of Strong Coupling Between Soil Moisture and  
759 Precipitation, *Science* (80-. ), 305(5687), 1138 LP-1140 [online] Available from:  
760 <http://science.sciencemag.org/content/305/5687/1138.abstract>, 2004.

761 Kollet SJ, Maxwell RM (2008) Capturing the influence of groundwater dynamics on land surface  
762 processes using an integrated, distributed watershed model. *Water Resour Res* 44:1–18. doi:  
763 10.1029/2007WR006004

764 Kurylyk, B. L. and MacQuarrie, K. T. B.: The uncertainty associated with estimating future  
765 groundwater recharge: A summary of recent research and an example from a small unconfined  
766 aquifer in a northern humid-continental climate, *J. Hydrol.*, 492, 244–253,  
767 doi:10.1016/j.jhydrol.2013.03.043, 2013.

768 Liu, C., Ikeda, K., Rasmussen, R., Barlage, M., Newman, A. J., Prein, A. F., Chen, F., Chen, L.,  
769 Clark, M., Dai, A., Dudhia, J., Eidhammer, T., Gochis, D., Gutmann, E., Kurkute, S., Li, Y.,  
770 Thompson, G. and Yates, D.: Continental-scale convection-permitting modeling of the current  
771 and future climate of North America, *Clim. Dyn.*, 49(1–2), 71–95, doi:10.1007/s00382-016-  
772 3327-9, 2017.

773 Martinez, J. A., Dominguez, F. and Miguez-Macho, G.: Effects of a Groundwater Scheme on the  
774 Simulation of Soil Moisture and Evapotranspiration over Southern South America, *J.*  
775 *Hydrometeorol.*, 17(11), 2941–2957, doi:10.1175/JHM-D-16-0051.1, 2016.

776 Maxwell RM, Miller NL (2005) Development of a Coupled Land Surface and Groundwater  
777 Model. 233–247

778 Maxwell, R. M. and Kollet, S. J.: Interdependence of groundwater dynamics and land-energy  
779 feedbacks under climate change, *Nat. Geosci.*, 1(10), 665–669, doi:10.1038/ngeo315, 2008.

780 [Maxwell, R. M., Condon, L. E. and Kollet, S. J.: A high-resolution simulation of groundwater and](#)  
781 [surface water over most of the continental US with the integrated hydrologic model ParFlow](#)  
782 [v3, \*Geosci. Model Dev.\*, 8\(3\), 923–937, doi:10.5194/gmd-8-923-2015, 2015.](#)

783 Meixner, T., Manning, A. H., Stonestrom, D. A., Allen, D. M., Ajami, H., Blasch, K. W.,  
784 Brookfield, A. E., Castro, C. L., Clark, J. F., Gochis, D. J., Flint, A. L., Neff, K. L., Niraula,  
785 R., Rodell, M., Scanlon, B. R., Singha, K. and Walvoord, M. A.: Implications of projected  
786 climate change for groundwater recharge in the western United States, *J. Hydrol.*, 534, 124–  
787 138, doi:10.1016/j.jhydrol.2015.12.027, 2016.

788 Miguez-Macho, G., Fan, Y., Weaver, C. P., Walko, R. and Robock, A.: Incorporating water table  
789 dynamics in climate modeling: 2. Formulation, validation, and soil moisture simulation, *J.*  
790 Miguez-Macho, G. and Fan, Y.: The role of groundwater in the Amazon water cycle: 1. Influence  
791 on seasonal streamflow, flooding and wetlands, *J. Geophys. Res. Atmos.*, 117(15), 1–30,  
792 doi:10.1029/2012JD017539, 2012.

793 Moeck, C., Brunner, P. and Hunkeler, D.: The influence of model structure on groundwater  
794 recharge rates in climate-change impact studies, *Hydrogeol. J.*, 24(5), 1171–1184,  
795 doi:10.1007/s10040-016-1367-1, 2016.

796 Mohammed, A. A., Kurylyk, B. L., Cey, E. E. and Hayashi, M.: Snowmelt Infiltration and  
797 Macropore Flow in Frozen Soils: Overview, Knowledge Gaps, and a Conceptual Framework,  
798 *Vadose Zo. J.*, 17(1), doi:10.2136/vzj2018.04.0084, 2018.

799 Musselman, K. N., Clark, M. P., Liu, C., Ikeda, K. and Rasmussen, R.: Slower snowmelt in a  
800 warmer world, *Nat. Clim. Chang.*, 7(February), 214–220, doi:10.1038/NCLIMATE3225,  
801 2017.

802 National Research Council: Groundwater fluxes across inter- faces. The National Academy Press,  
803 85 pp, 2003

804 Niraula R, Meixner T, Dominguez F, et al (2017) How Might Recharge Change Under Projected  
805 Climate Change in the Western U.S.? *Geophys Res Lett* 44:10,407-10,418. doi:  
806 10.1002/2017GL075421

807 Niu, G.-Y., & Yang, Z.-L. (2006). Effects of Frozen Soil on Snowmelt Runoff and Soil Water  
808 Storage at a Continental Scale. *Journal of Hydrometeorology*, 7(5), 937–952.  
809 <https://doi.org/10.1175/JHM538.1>

810 Niu G, Yang Z, Dickinson RE, Gulden LE (2007) Development of a simple groundwater model  
811 for use in climate models and evaluation with Gravity Recovery and Climate Experiment  
812 data. 112:1–14. doi: 10.1029/2006JD007522

813 Niu, G. Y., Yang, Z. L., Mitchell, K. E., Chen, F., Ek, M. B., Barlage, M., Kumar, A., Manning,  
814 K., Niyogi, D., Rosero, E., Tewari, M. and Xia, Y.: The community Noah land surface model  
815 with multiparameterization options (Noah-MP): 1. Model description and evaluation with  
816 local-scale measurements, *J. Geophys. Res. Atmos.*, 116(12), 1–19,  
817 doi:10.1029/2010JD015139, 2011.

818 Niu G-Y, Zeng X (2012) Earth System Model, Modeling the Land Component of. In: *Climate*  
819 *Change Modeling Methodology*. Springer New York, New York, NY, pp 139–168

820 Pokhrel, Y. N., Fan, Y., Miguez-Macho, G., Yeh, P. J. F. and Han, S. C.: The role of groundwater  
821 in the Amazon water cycle: 3. Influence on terrestrial water storage computations and  
822 comparison with GRACE, *J. Geophys. Res. Atmos.*, 118(8), 3233–3244,  
823 doi:10.1002/jgrd.50335, 2013.

824 Pokhrel, Y. N., Fan, Y. and Miguez-Macho, G.: Potential hydrologic changes in the Amazon by  
825 the end of the 21st century and the groundwater buffer, *Environ. Res. Lett.*, 9(8),  
826 doi:10.1088/1748-9326/9/8/084004, 2014.

827 Pomeroy, J. W.: The cold regions hydrological model: a platform for basing process representation  
828 and model structure on physical evidence, *Hydrol. Process.*, 21, 2650–2667, doi:10.1002/hyp,  
829 2007.

830 Prein, A. F., Gobiet, A., Suklitsch, M., Truhetz, H., Awan, N. K., Keuler, K. and Georgievski, G.:  
831 Added value of convection permitting seasonal simulations, , 2655–2677,  
832 doi:10.1007/s00382-013-1744-6, 2013.

833 Prein, A. F., Langhans, W., Fossier, G., Ferrone, A., Ban, N., Goergen, K., Keller, M., Tölle, M.,  
834 Gutjahr, O., Feser, F., Brisson, E., Kollet, S., Schmidli, J., Van Lipzig, N. P. M. and Leung,  
835 R.: A review on regional convection-permitting climate modeling: Demonstrations, prospects,  
836 and challenges, *Rev. Geophys.*, 53(2), 323–361, doi:10.1002/2014RG000475, 2015.

837 Rasmussen, K. L., Prein, A. F., Rasmussen, R. M., Ikeda, K. and Liu, C.: Changes in the convective  
838 population and thermodynamic environments in convection-permitting regional climate  
839 simulations over the United States, *Clim. Dyn.*, (0123456789), 1–26, doi:10.1007/s00382-  
840 017-4000-7, 2017.

841 Remenda VH, van der Kamp G, Cherry JA (1996) Use of vertical profiles of • 180 to constrain  
842 estimates of hydraulic conductivity in a thick, unfractured aquitard. 32:2979–2987

843 Shangguan W, Dai Y, Duan Q, et al (2014) *Journal of Advances in Modeling Earth Systems*. J  
844 *Adv Model Earth Syst* 6:249–263. doi: 10.1002/2013MS000293. Received

845 Sherwood, S. C., Bony, S. and Dufresne, J.: Spread in model climate sensitivity traced to  
846 atmospheric convective mixing, , doi:10.1038/nature12829, 2014.

847 Siebert, S., Burke, J., Faures, J. M., Frenken, K., Hoogeveen, J., Döll, P. and Portmann, F. T.:  
848 Groundwater use for irrigation - A global inventory, *Hydrol. Earth Syst. Sci.*, 14(10), 1863–  
849 1880, doi:10.5194/hess-14-1863-2010, 2010.

850 Smerdon, B. D.: A synopsis of climate change effects on groundwater recharge, *J. Hydrol.*, 555,  
851 125–128, doi:10.1016/j.jhydrol.2017.09.047, 2017.

852 Statistics Canada: Quarterly Estimates of the Population of Canada, the Provinces and the  
853 Territories, 11-3, Catalogue 91-001, Ottawa, 1996

854 Taylor, R. G.: Ground water and climate change, , 3(November 2012),  
855 doi:10.1038/NCLIMATE1744, 2013.

856 Tremblay, L., Larocque, M., Anctil, F. and Rivard, C.: Teleconnections and interannual variability  
857 in Canadian groundwater levels, *J. Hydrol.*, 410(3–4), 178–188,  
858 doi:10.1016/j.jhydrol.2011.09.013, 2011.

859 UNESCO: *Groundwater Resources of the World and Their Use*, edited by I. Zektser and L. Everett,  
860 Paris., 2004.

861 Van Der Kamp G, Hayashi M (2009) Groundwater-wetland ecosystem interaction in the  
862 semiarid glaciated plains of North America. *Hydrogeol J* 17:203–214. doi: 10.1007/s10040-  
863 008-0367-1

864 Xue Y, Sellers PJ, Kinter JL, Shukla J (1991) A Simplified Biosphere Model for Global Climate  
865 Studies. *J Clim* 4:345–364. doi: 10.1175/1520-0442(1991)004<0345:ASBMFG>2.0.CO;2

866 Yang, Z. L., Niu, G. Y., Mitchell, K. E., Chen, F., Ek, M. B., Barlage, M., Longuevergne, L.,  
867 Manning, K., Niyogi, D., Tewari, M. and Xia, Y.: The community Noah land surface model  
868 with multiparameterization options (Noah-MP): 2. Evaluation over global river basins, *J.*  
869 *Geophys. Res. Atmos.*, 116(12), 1–16, doi:10.1029/2010JD015140, 2011.

Deleted: ¶

\*\*\*\*\*Page Break\*\*\*\*\*

¶

873 Table and Figure

874

875 **Table 1.** Summary of the locations and aquifer type and soil type of the 33 selected wells.

Site Name/ Site No.	Lat	Lon	Elev	Aquifer type	Aquifer Lithology	Model Elevation	Model Soil type
Devon 0162	53.41	-113.76	700.0	Unconfined	Sand	697.366	Sandy loam
Hardisty 0143	52.67	-111.31	622.0	Unconfined	Gravel	633.079	Loam
Kirkpatrick Lake 0229	51.95	-111.44	744.5	Semi-confined	Sandstone	778.311	Sandy loam
Metiskow 0267	52.42	-110.60	677.5	Unconfined	Sand	679.516	Loamy sand
Wagner 0172	53.56	-113.82	670.0	Surficial	Sand	670.845	Silt loam
Narrow Lake 252	54.60	-113.63	640.0	Unconfined	Sand	701.0	Clay loam
Baldon 060	50.25	-105.50	590.184	Surficial	-	580.890	Sandy loam
Beauval	55.11	-107.74	434.3	Intertill	Sand	446.5	Sandy loam
Blucher	52.03	-106.20	521.061	Intertill	Sand/Gravel	523.217	Loam
Crater Lake	50.95	-102.46	524.158	Intertill	Sand/Gravel/Clay	522.767	Loam
Duck Lake	52.92	-106.23	502.920	Surficial	Sand	501.729	Loamy sand
Forget	49.70	-102.85	606.552	Surficial	Sand	605.915	Sandy loam
Garden Head	49.74	-108.52	899.160	Bedrock	Sand/Till	894.357	Clay loam
Nokomis	51.51	-105.06	516.267	Bedrock	Sand	511.767	Clay loam
Shaunavon	49.69	-108.50	896.040	Bedrock	Sand/Till	900.433	Clay loam
Simpson 13	51.45	-105.18	496.620	Surficial	Sand	493.313	Sandy loam
Simpson 14	51.457	-105.19	496.600	Surficial	Sand	493.313	Sandy loam
Yorkton 517	51.17	-102.50	513.643	Surficial	Sand/Gravel	511.181	Loam
Agrium 43	52.03	-107.01	500.229	Intertill	Sand	510.771	Loam
460120097591803	46.02	-97.98	401.177	Alluvial	Sand/Gravel	400.381	Sandy loam
461838097553402	46.31	-97.92	401.168	-	Sand/Gravel	404.719	Clay loam
462400097552502	46.39	-97.92	409.73	-	Sand/Gravel	407.405	Sandy loam
462633097163402	46.44	-97.27	325.52	Alluvial	Sand/Gravel	323.728	Sandy loam
463422097115602	46.57	-97.19	320.40	Alluvial	Sand/Gravel	314.167	Sandy loam
464540100222101	46.76	-100.37	524.91	-	Sand/Gravel	522.600	Clay loam
473841096153101	47.64	-96.25	351.77	Surficial	Sand/Gravel	344.180	Loamy sand
473945096202402	47.66	-96.34	327.78	Surficial	Sand/Gravel	328.129	Sandy loam
474135096203001	47.69	-96.34	325.97	Surficial	Sand/Gravel	327.764	Sandy loam
474436096140801	47.74	-96.23	341.90	Surficial	Sand/Gravel	336.210	Sandy loam
475224098443202	47.87	-98.74	451.33	-	Sand/Gravel	450.463	Sandy loam
481841097490301	48.31	-97.81	355.61	-	Sand/Gravel	359.568	Clay loam
482212099475801	48.37	-99.79	488.65	-	Sand/Gravel	488.022	Sandy loam
CRN Well WLN03	45.98	-95.20	410.7	Surficial	Sand/Gravel	411.4	Sandy loam

876

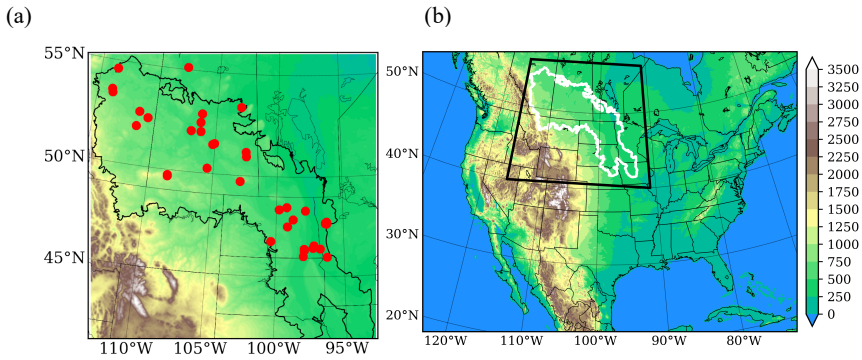
877 **Table 2.** Summary of mean and standard deviation (std) of WTD from 33 groundwater wells, from  
878 observation records (OBS), default model (CTRL) and replacing with sand soil simulation (REP).  
879 Bold texts indicate improvement in the REP than the CTRL run.  
880

Site Name/Number	OBS_mean	CTRL_mean	REP_mean	OBS_std	CTRL_std	REP_std
Devon 0162	-2.46	-2.69	<b>-2.38</b>	0.43	0.45	0.09
Hardisty 0143	-2.44	-8.91	<b>-6.88</b>	0.41	0.64	<b>0.36</b>
Kirkpatrick Lake 0229	-4.22	-4.03	-3.45	0.43	0.98	<b>0.22</b>
Metiskow 0267	-2.54	-5.39	<b>-4.43</b>	0.34	0.78	<b>0.55</b>
Narrow Lake 252	-2.31	-4.81	<b>-3.75</b>	0.28	0.60	0.51
Wagner 0172	-2.14	-8.06	<b>-2.70</b>	0.48	0.37	0.21
Baildon 060	-2.80	-3.29	<b>-3.20</b>	0.47	0.58	0.30
Beauval	-3.78	-4.85	<b>-4.20</b>	0.44	0.56	0.32
Blucher	-2.20	-4.24	<b>-2.16</b>	0.3	0.92	<b>0.26</b>
Crater Lake	-4.33	-3.97	-3.64	1.1	0.4	0.28
Duck Lake	-3.65	-3.69	-3.17	0.54	0.41	<b>0.62</b>
Forget	-2.28	-2.37	<b>-2.23</b>	0.33	0.17	0.19
Garden Head	-3.67	-4.85	<b>-3.77</b>	0.88	0.70	0.30
Nokomis	-1.04	-2.70	<b>-2.17</b>	0.23	0.55	<b>0.17</b>
Shaunavon	-1.62	-4.41	<b>-2.58</b>	0.42	0.69	0.20
Simpson 13	-4.82	-4.83	-3.02	0.31	0.91	<b>0.17</b>
Simpson 14	-2.03	-2.61	<b>-1.82</b>	0.34	0.18	<b>0.27</b>
Yorkton 517	-2.87	-3.97	<b>-1.98</b>	0.8	0.46	0.32
Agrium 43	-2.66	-3.75	<b>-3.38</b>	0.32	1.05	<b>0.36</b>
460120097591803	-1.44	-2.33	<b>-1.63</b>	0.56	0.24	<b>0.50</b>
461838097553402	-1.17	-2.32	<b>-1.68</b>	0.27	0.24	0.43
462400097552502	-4.9	-5.61	<b>-5.37</b>	0.29	0.09	<b>0.17</b>
462633097163402	-1.18	-1.49	<b>-1.02</b>	0.46	0.29	<b>0.54</b>
463422097115602	-1.36	-2.28	<b>-1.66</b>	0.34	0.23	0.49
464540100222101	-2.02	-3.64	<b>-2.78</b>	0.52	0.43	0.32
473841096153101	-0.77	-1.48	<b>-1.37</b>	0.24	0.18	0.51
473945096202402	-1.59	-1.58	-1.56	0.32	0.24	0.51
474135096203001	-0.72	-1.48	<b>-1.30</b>	0.33	0.25	0.54
474436096140801	-2.44	-2.29	-1.96	0.39	0.21	<b>0.40</b>
475224098443202	-4.52	-4.28	-5.31	0.75	0.52	0.34
481841097490301	-4.39	-4.24	-4.58	0.79	0.28	0.17
482212099475801	-2.13	-2.32	<b>-2.26</b>	0.24	0.20	0.17
CRN WLN 03	-2.04	-2.18	-1.88	0.24	0.18	0.43

881  
882



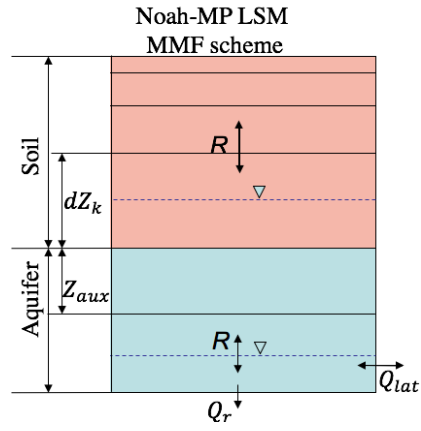
883  
884



885  
886  
887  
888  
889

**Fig. 1** (a) Topography of the Prairie Pothole Region (PPR; black outline) and groundwater wells (red dots); (b) Topography of the WRF CONUS domain, the black box indicates the PPR domain.

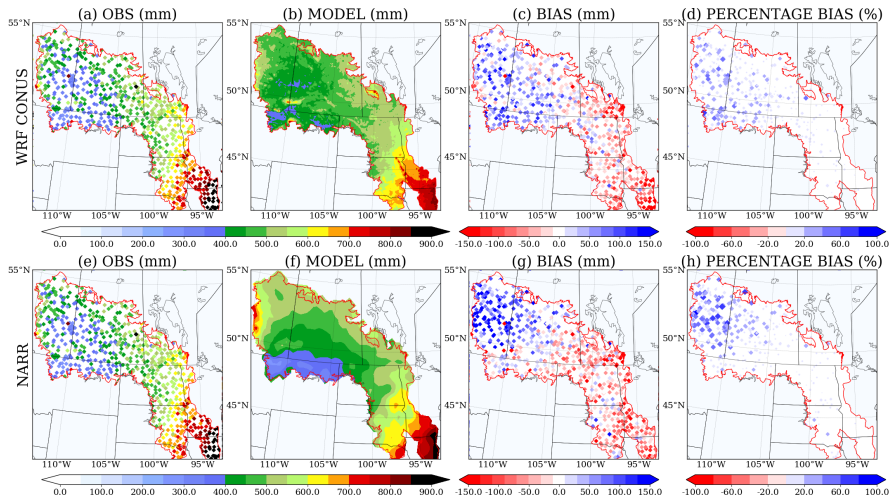
890



891

892 **Fig. 2** Structure of the Noah-MP LSM coupled with MMF groundwater scheme, the top 2-m soil of 4 layers whose thicknesses  
893 are 0.1, 0.3, 0.6 and 1.0 m. An unconfined aquifer is added below the 2-m boundary, including an auxiliary layer and the saturated  
894 aquifer. Positive flux of  $R$  denotes downward flow. Two water tables are shown, one within the 2-m soil and one below,  
895 indicating that the model is capable to deal with both shallow and deep water table.  
896  
897

898



899

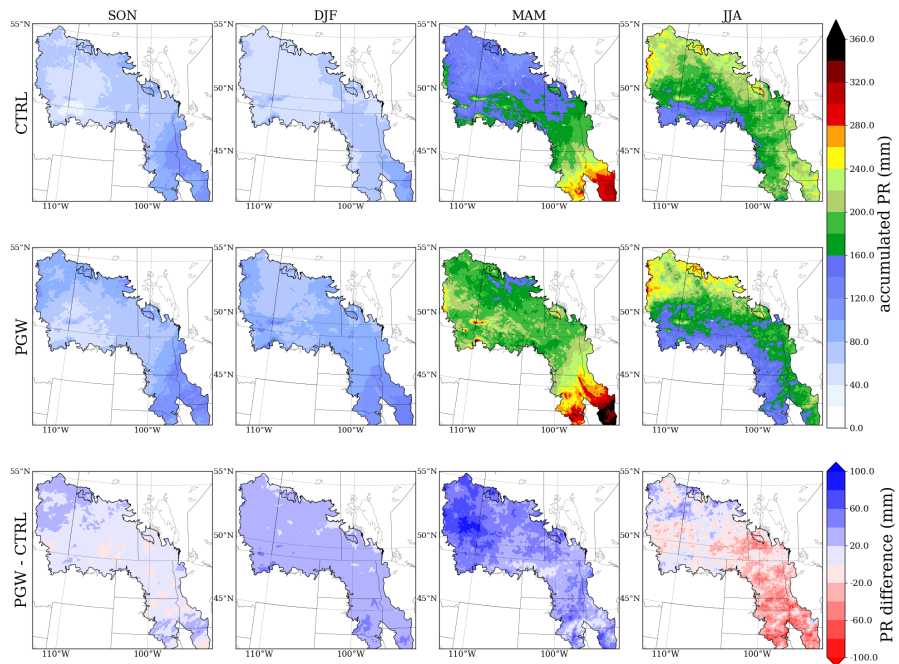
900

901

902

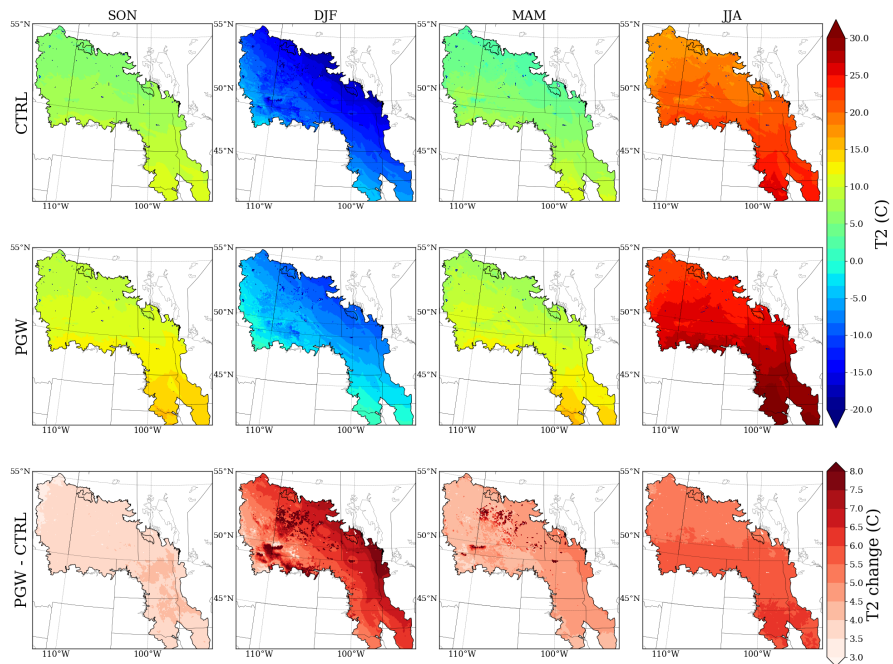
903

**Fig. 3** Evaluation of the annual precipitation from two model products (b, f), WRF CONUS and NARR against rain gauge observation (a, e), their bias (c, g) and percentage bias (d, h).



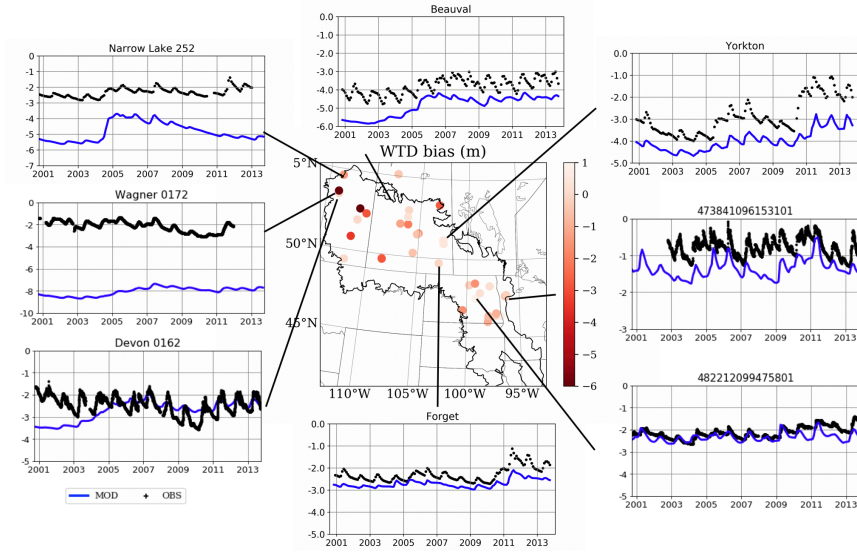
904  
905  
906  
907

**Fig. 4** Seasonal Accumulated precipitation from current climate (CTRL, top), future climate (PGW, middle) and projected change (PGW-CTRL, bottom) in forcing data.



908  
 909 **Fig. 5** Seasonal temperatures from current climate (CTRL, top), future climate (PGW, middle) and projected  
 910 change (PGW-CTRL, bottom) in forcing data.  
 911

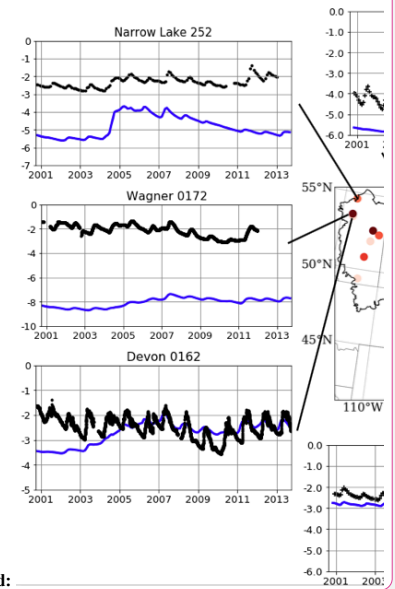
912



913  
914  
915  
916  
917  
918

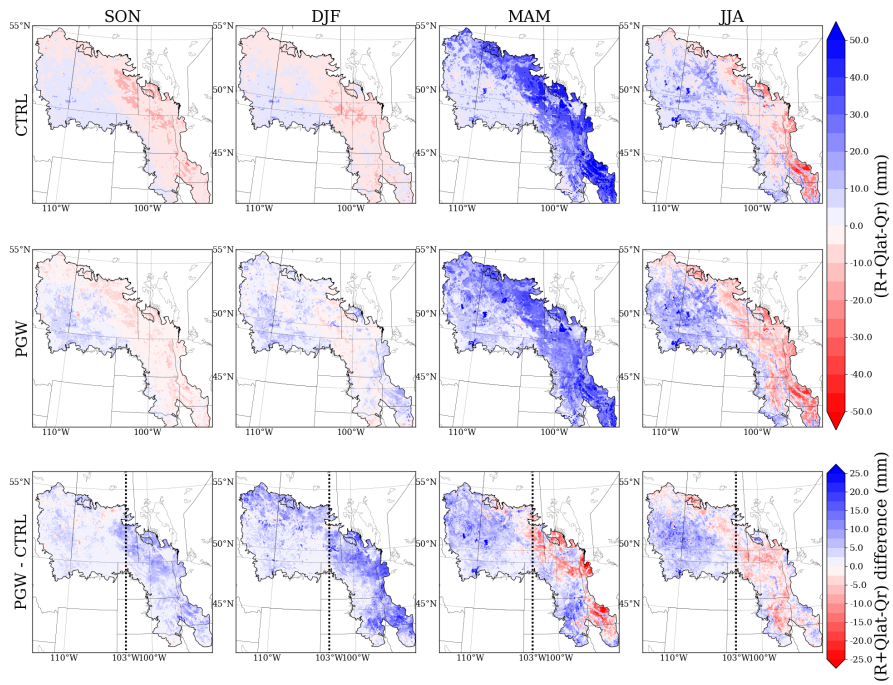
**Fig. 6.** WTD (m) bias from CTRL simulation and timeseries from 8 groundwater wells in PPR (black for observation and blue for CTRL model simulation). See Table 2 CTRL column for the model statistics and supplemental materials for complete timeseries from 33 wells.

Formatted: Centered



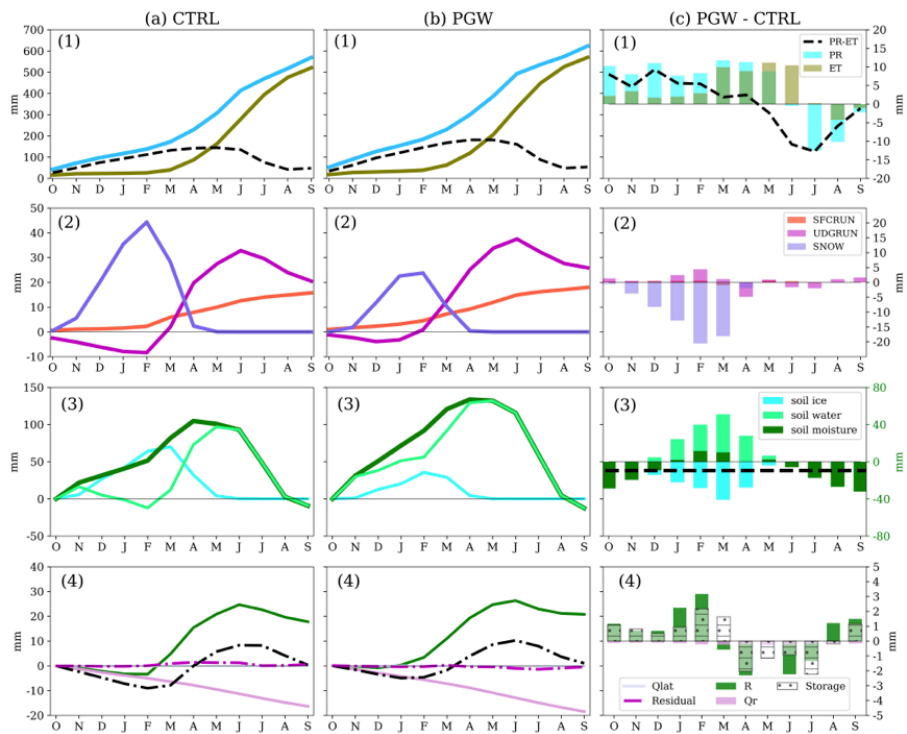
Deleted:

Formatted: Font: 10 pt



920  
921  
922  
923  
924

**Fig. 7** Seasonal accumulated total groundwater fluxes ( $R+Q_{lat} - Q_r$ ) for current climate (CTRL, top), future climate (PGW, middle) and projected change (PGW-CTRL, bottom) in forcing data. Black dashed lines in PGW-CTRL separate the PPR into eastern and western halves.



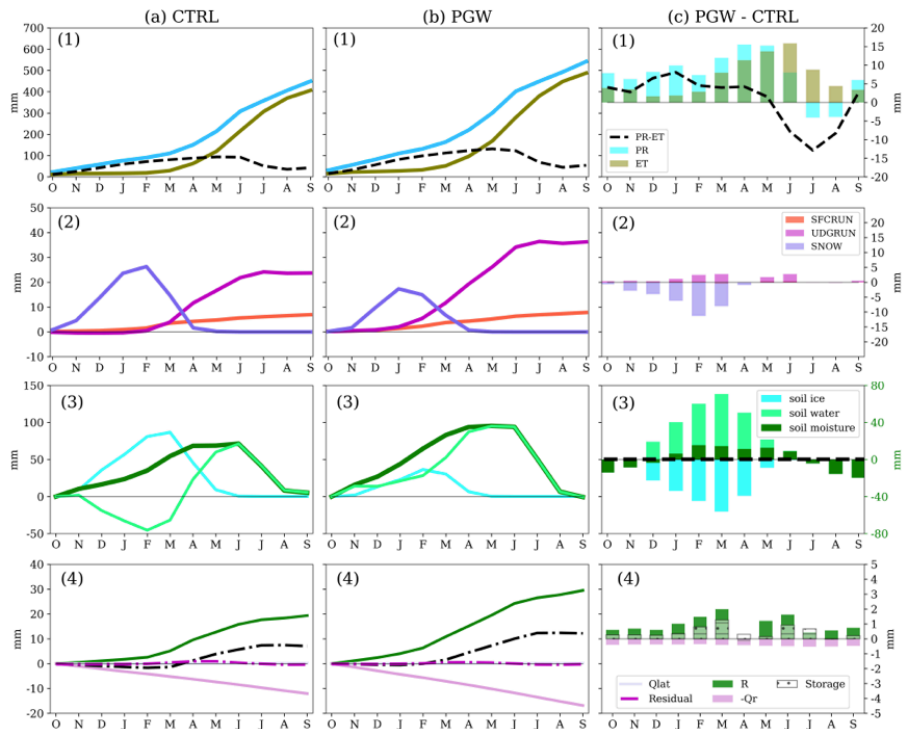
storage change: 1.763 mm  
 recharge change: 4.152 mm  
 river flux change: 2.260 mm  
 lateral flux change: -0.001 mm

925  
 926  
 927  
 928  
 929  
 930  
 931  
 932  
 933  
 934

**Fig. 8** Water budget analysis in the eastern PPR in (a) CTRL, (b) PGW and (c) PGW – CTRL. Water budget terms include: (1) *PR* & *ET*, (2) surface snow, surface runoff and underground runoff (*SNOW*, *SFCRUN*, and *UDGRUN*), (3) change of soil moisture storage (soil water, soil ice and total soil moisture,  $\Delta SMC$ ) and (4) groundwater fluxes and the change of groundwater storage ( $R$ ,  $Q_{lat}$ ,  $Q_r$ ,  $\Delta S_g$ ). The annual mean soil moisture change (PGW-CTRL) is shown with black dashed line in (3). The Residual term is defined as  $Res = (R + Q_{lat} - Q_r) - \Delta S_g$  in (4). Note that in (a) and (b) the accumulated fluxes and change in storage are shown in lines, whereas in (c) the difference in (PGW-CTRL) is shown for each individual month in bars.

Formatted: Font: Bold





storage change: 5.390 mm  
 recharge change: 10.727 mm  
 river flux change: 5.207 mm  
 lateral flux change: 0.000 mm

935

936

937

938

939

940

941

942

943

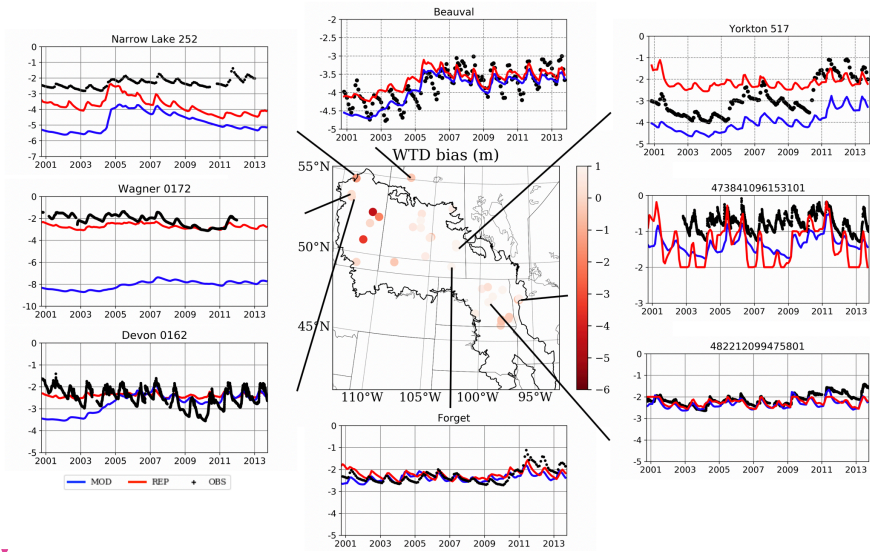
944

945

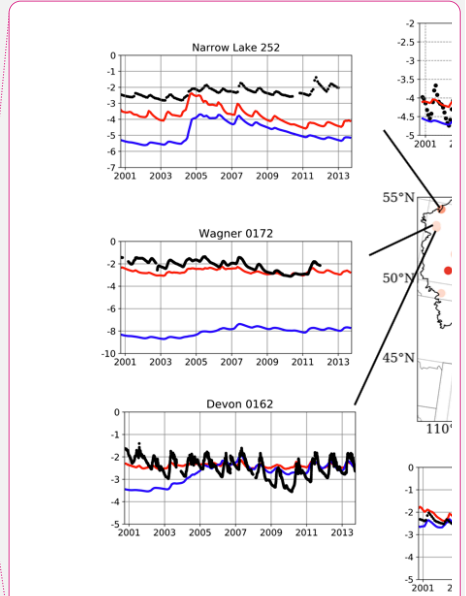
**Fig. 9** Same as Fig. 8. Water budget analysis in the western PPR: in (a) CTRL, (b) PGW and (c) PGW – CTRL. Water budget terms include: (1) PR & ET, (2) surface snow, surface runoff and underground runoff (SNOW, SFCRUN, and UDGRUN), (3) change of soil moisture storage (soil water, soil ice and total soil moisture,  $\Delta SMC$ ) and (4) groundwater fluxes and the change of groundwater storage ( $R, Q_{lat}, Q_r, \Delta S_g$ ). The annual mean soil moisture change (PGW-CTRL) is shown with black dashed line in (3). The Residual term is defined as  $Res = (R + Q_{lat} - Q_r) - \Delta S_g$  in (4). Note that in (a) and (b) the accumulated fluxes and change in storage are shown in lines, whereas in (c) the difference in (PGW-CTRL) is shown for each individual month in bars.

Deleted: , but for the western PPR.  
 Formatted: Font: Bold

Formatted: Font: Not Bold



947  
 948 **Fig. 10** Same as Fig. 6, **WTD (m) bias from CTRL simulation and timeseries from 8 groundwater wells in PPR** (black for  
 949 **observation and blue for CTRL model simulation, and red for the replacing soil type simulation**). REP is the additional  
 950 simulation by replacing the default soil type in the model with sandy soil type.  
 951  
 952  
 953



Deleted:

Formatted: Centered

Formatted: Font: 10 pt

Deleted: the timeseries of simulated WTD from both default model (blue) and replacing soil type simulation, REP (red)

Formatted: Font: 10 pt

Formatted: Font: Not Bold

Page 12: [1] Formatted Zhang, Zhe 11/22/19 3:33:00 PM

Font: 12 pt

Page 12: [1] Formatted Zhang, Zhe 11/22/19 3:33:00 PM

Font: 12 pt

Page 12: [1] Formatted Zhang, Zhe 11/22/19 3:33:00 PM

Font: 12 pt

Page 12: [1] Formatted Zhang, Zhe 11/22/19 3:33:00 PM

Font: 12 pt

Page 12: [1] Formatted Zhang, Zhe 11/22/19 3:33:00 PM

Font: 12 pt

Page 12: [1] Formatted Zhang, Zhe 11/22/19 3:33:00 PM

Font: 12 pt

Page 12: [2] Formatted Zhang, Zhe 11/22/19 3:33:00 PM

Font: 12 pt

Page 12: [2] Formatted Zhang, Zhe 11/22/19 3:33:00 PM

Font: 12 pt

Page 12: [2] Formatted Zhang, Zhe 11/22/19 3:33:00 PM

Font: 12 pt

Page 12: [2] Formatted Zhang, Zhe 11/22/19 3:33:00 PM

Font: 12 pt

Page 12: [2] Formatted Zhang, Zhe 11/22/19 3:33:00 PM

Font: 12 pt

Page 12: [2] Formatted Zhang, Zhe 11/22/19 3:33:00 PM

Font: 12 pt

Page 12: [2] Formatted Zhang, Zhe 11/22/19 3:33:00 PM

Font: 12 pt

Page 12: [2] Formatted Zhang, Zhe 11/22/19 3:33:00 PM

Font: 12 pt

Page 12: [2] Formatted Zhang, Zhe 11/22/19 3:33:00 PM

Font: 12 pt

Page 12: [2] Formatted Zhang, Zhe 11/22/19 3:33:00 PM

Font: 12 pt

Page 12: [2] Formatted Zhang, Zhe 11/22/19 3:33:00 PM

Font: 12 pt

Page 12: [2] Formatted Zhang, Zhe 11/22/19 3:33:00 PM

Font: 12 pt

Page 12: [2] Formatted Zhang, Zhe 11/22/19 3:33:00 PM

Font: 12 pt

Page 12: [2] Formatted Zhang, Zhe 11/22/19 3:33:00 PM

Font: 12 pt

Page 12: [2] Formatted Zhang, Zhe 11/22/19 3:33:00 PM

Font: 12 pt

Page 12: [2] Formatted Zhang, Zhe 11/22/19 3:33:00 PM

Font: 12 pt

Page 12: [3] Formatted Zhang, Zhe 11/22/19 3:33:00 PM

Font: 12 pt

Page 12: [3] Formatted Zhang, Zhe 11/22/19 3:33:00 PM

Font: 12 pt

Page 12: [3] Formatted Zhang, Zhe 11/22/19 3:33:00 PM

Font: 12 pt

Page 12: [3] Formatted Zhang, Zhe 11/22/19 3:33:00 PM

Font: 12 pt

Page 12: [3] Formatted Zhang, Zhe 11/22/19 3:33:00 PM

Font: 12 pt

Page 12: [3] Formatted Zhang, Zhe 11/22/19 3:33:00 PM

Font: 12 pt

Page 12: [3] Formatted Zhang, Zhe 11/22/19 3:33:00 PM

Font: 12 pt

Page 12: [3] Formatted Zhang, Zhe 11/22/19 3:33:00 PM

Font: 12 pt

Page 12: [3] Formatted Zhang, Zhe 11/22/19 3:33:00 PM

Font: 12 pt

Page 12: [3] Formatted Zhang, Zhe 11/22/19 3:33:00 PM

Font: 12 pt

Page 12: [3] Formatted Zhang, Zhe 11/22/19 3:33:00 PM

Font: 12 pt

Page 12: [3] Formatted Zhang, Zhe 11/22/19 3:33:00 PM

Font: 12 pt

Page 12: [3] Formatted Zhang, Zhe 11/22/19 3:33:00 PM

Font: 12 pt

Page 12: [3] Formatted Zhang, Zhe 11/22/19 3:33:00 PM

Font: 12 pt

Page 12: [4] Formatted Zhang, Zhe 11/22/19 3:33:00 PM

Font: 12 pt

Page 12: [4] Formatted Zhang, Zhe 11/22/19 3:33:00 PM

Font: 12 pt

▲ Page 12: [4] Formatted Zhang, Zhe 11/22/19 3:33:00 PM

Font: 12 pt

▲ Page 12: [4] Formatted Zhang, Zhe 11/22/19 3:33:00 PM

Font: 12 pt

▲ Page 12: [4] Formatted Zhang, Zhe 11/22/19 3:33:00 PM

Font: 12 pt

▲ Page 12: [4] Formatted Zhang, Zhe 11/22/19 3:33:00 PM

Font: 12 pt

▲ Page 12: [4] Formatted Zhang, Zhe 11/22/19 3:33:00 PM

Font: 12 pt

▲ Page 12: [4] Formatted Zhang, Zhe 11/22/19 3:33:00 PM

Font: 12 pt

▲ Page 12: [4] Formatted Zhang, Zhe 11/22/19 3:33:00 PM

Font: 12 pt

▲ Page 12: [4] Formatted Zhang, Zhe 11/22/19 3:33:00 PM

Font: 12 pt

▲ Page 12: [4] Formatted Zhang, Zhe 11/22/19 3:33:00 PM

Font: 12 pt

▲ Page 12: [4] Formatted Zhang, Zhe 11/22/19 3:33:00 PM

Font: 12 pt

▲ Page 12: [4] Formatted Zhang, Zhe 11/22/19 3:33:00 PM

Font: 12 pt

▲ Page 12: [4] Formatted Zhang, Zhe 11/22/19 3:33:00 PM

Font: 12 pt

▲ Page 12: [4] Formatted Zhang, Zhe 11/22/19 3:33:00 PM

Font: 12 pt

▲ Page 12: [5] Formatted Zhang, Zhe 11/22/19 3:33:00 PM

Font: 12 pt

▲ Page 12: [5] Formatted Zhang, Zhe 11/22/19 3:33:00 PM

Font: 12 pt

▲ Page 12: [6] Formatted Zhang, Zhe 11/22/19 3:33:00 PM

Font: 12 pt

▲ Page 12: [6] Formatted Zhang, Zhe 11/22/19 3:33:00 PM

Font: 12 pt

▲ Page 12: [7] Formatted Zhang, Zhe 11/22/19 3:33:00 PM

Font: 12 pt

▲

Page 12: [7] Formatted Zhang, Zhe 11/22/19 3:33:00 PM

Font: 12 pt

Page 12: [7] Formatted Zhang, Zhe 11/22/19 3:33:00 PM

Font: 12 pt

Page 12: [7] Formatted Zhang, Zhe 11/22/19 3:33:00 PM

Font: 12 pt

Page 12: [7] Formatted Zhang, Zhe 11/22/19 3:33:00 PM

Font: 12 pt

Page 12: [7] Formatted Zhang, Zhe 11/22/19 3:33:00 PM

Font: 12 pt

Page 12: [7] Formatted Zhang, Zhe 11/22/19 3:33:00 PM

Font: 12 pt

Page 12: [7] Formatted Zhang, Zhe 11/22/19 3:33:00 PM

Font: 12 pt

Page 12: [7] Formatted Zhang, Zhe 11/22/19 3:33:00 PM

Font: 12 pt

Page 12: [7] Formatted Zhang, Zhe 11/22/19 3:33:00 PM

Font: 12 pt

Page 12: [7] Formatted Zhang, Zhe 11/22/19 3:33:00 PM

Font: 12 pt

Page 12: [7] Formatted Zhang, Zhe 11/22/19 3:33:00 PM

Font: 12 pt

Page 12: [7] Formatted Zhang, Zhe 11/22/19 3:33:00 PM

Font: 12 pt

Page 12: [7] Formatted Zhang, Zhe 11/22/19 3:33:00 PM

Font: 12 pt

Page 12: [7] Formatted Zhang, Zhe 11/22/19 3:33:00 PM

Font: 12 pt

Page 12: [7] Formatted Zhang, Zhe 11/22/19 3:33:00 PM

Font: 12 pt

Page 12: [7] Formatted Zhang, Zhe 11/22/19 3:33:00 PM

Font: 12 pt

Page 12: [7] Formatted Zhang, Zhe 11/22/19 3:33:00 PM

Font: 12 pt

Page 12: [7] Formatted Zhang, Zhe 11/22/19 3:33:00 PM

Font: 12 pt

Page 12: [7] Formatted Zhang, Zhe 11/22/19 3:33:00 PM

Font: 12 pt

▲ Page 12: [7] Formatted Zhang, Zhe 11/22/19 3:33:00 PM

Font: 12 pt

▲ Page 12: [7] Formatted Zhang, Zhe 11/22/19 3:33:00 PM

Font: 12 pt

▲ Page 12: [7] Formatted Zhang, Zhe 11/22/19 3:33:00 PM

Font: 12 pt

▲ Page 12: [7] Formatted Zhang, Zhe 11/22/19 3:33:00 PM

Font: 12 pt

▲ Page 12: [8] Formatted Zhang, Zhe 11/22/19 3:33:00 PM

Font: 12 pt

▲ Page 12: [8] Formatted Zhang, Zhe 11/22/19 3:33:00 PM

Font: 12 pt

▲ Page 12: [9] Formatted Zhang, Zhe 11/22/19 3:33:00 PM

Font: 12 pt

▲ Page 12: [9] Formatted Zhang, Zhe 11/22/19 3:33:00 PM

Font: 12 pt

▲ Page 12: [9] Formatted Zhang, Zhe 11/22/19 3:33:00 PM

Font: 12 pt

▲ Page 12: [9] Formatted Zhang, Zhe 11/22/19 3:33:00 PM

Font: 12 pt

▲ Page 12: [10] Formatted Zhang, Zhe 11/22/19 3:33:00 PM

Font: 12 pt

▲ Page 12: [10] Formatted Zhang, Zhe 11/22/19 3:33:00 PM

Font: 12 pt

▲ Page 12: [11] Formatted Zhang, Zhe 11/22/19 3:33:00 PM

Font: 12 pt

▲ Page 12: [11] Formatted Zhang, Zhe 11/22/19 3:33:00 PM

Font: 12 pt

▲ Page 12: [12] Formatted Zhang, Zhe 11/22/19 3:33:00 PM

Font: 12 pt

▲ Page 12: [12] Formatted Zhang, Zhe 11/22/19 3:33:00 PM

Font: 12 pt

▲